FINAL REPORT

EIGENVALUE ASSIGNMENT STRATEGIES IN ROTOR SYSTEMS

by

John N. Youngblood
Professor of Mechanical Engineering
The University of Alabama

and

Kenneth J. Welzyn
Graduate Assistant
Department of Mechanical Engineering
The University of Alabama

Prepared for

THE UNIVERSITY OF ALABAMA
COLLEGE OF ENGINEERING

The College of Engineering at The University of Alabama has an undergraduate enrollment of more than 2,300 students and a graduate enrollment exceeding 180. There are approximately 100 faculty members, a significant number of whom conduct research in addition to teaching.

Research is an integral part of the educational program, and research interests of the faculty parallel academic specialities. A wide variety of projects are included in the overall research effort of the College, and these projects form a solid base for the graduate program which offers fourteen different master's and five different doctor of philosophy degrees.

Other organizations on the University campus that contribute to particular research needs of the College of Engineering are the Charles L. Seebeck Computer Center, Geological Survey of Alabama, Marine Environmental Sciences Consortium, Mineral Resources Institute—State Mine Experiment Station, Mineral Resources Research Institute, Natural Resources Center, School of Mines and Energy Development, Tuscaloosa Metallurgy Research Center of the U.S. Bureau of Mines, and the Research Grants Committee.

This University community provides opportunities for interdisciplinary work in pursuit of the basic goals of teaching, research, and public service.

BUREAU OF ENGINEERING RESEARCH

The Bureau of Engineering Research (BER) is an integral part of the College of Engineering of The University of Alabama. The primary functions of the BER include: 1) identifying sources of funds and other outside support bases to encourage and promote the research and educational activities within the College of Engineering; 2) organizing and promoting the research interests and accomplishments of the engineering faculty and students; 3) assisting in the preparation, coordination, and execution of proposals, including research, equipment, and instructional proposals; 4) providing engineering faculty, students, and staff with services such as graphics and audiovisual support and typing and editing of proposals and scholarly works; 5) promoting faculty and staff development through travel and seed project support, incentive stipends, and publicity related to engineering faculty, students, and programs; 6) developing innovative methods by which the College of Engineering can increase its effectiveness in providing high quality educational opportunities for those with whom it has contact; and 7) providing a source of timely and accurate data that reflect the variety and depth of contributions made by the faculty, students, and staff of the College of Engineering to the overall success of the University in meeting its mission.

Through these activities, the BER serves as a unit dedicated to assisting the College of Engineering faculty by providing significant and quality service activities.

EIGENVALUE ASSIGNMENT STRATEGIES IN ROTOR SYSTEMS

by

John N. Youngblood
Professor of Mechanical Engineering
The University of Alabama

and

Kenneth J. Welzyn
Graduate Assistant
Department of Mechanical Engineering
The University of Alabama

PREFACE

This report documents the work done on NASA Grant NAG8034
to establish the control and direction of effective eigenvalue
excursions of lightly damped, speed dependent rotor systems
using passive control. Both second order and sixth order
bi-axis, quasi-linear, speed dependent generic models were
investigated. In every case a single, bi-directional control
bearing was used in a passive feedback stabilization loop to
resist modal destabilization above the rotor critical speed.

Assuming incomplete state measurement, sub-optimal control
strategies were used to define the preferred location of the
control bearing, the most effective measurement locations, and
the best set of control gains to extend the speed range of
stable operation. Speed dependent control gains were found by
Powell's method to maximize the minimum modal damping ratio
for the speed dependent linear model. An increase of 300
percent in stable speed operation was obtained for the
sixth order linear system using passive control.

Simulations were run to examine the effectiveness of the
linear control law on nonlinear rotor models with bearing
deadband. The maximum level of control effort (force)
required by the control bearing to stabilize the rotor at
speeds above the critical was determined for the models with
bearing deadband.

TABLE OF CONTENTS

LIST OF TABLES

LIST OF FIGURES

CHAPTER I

INTRODUCTION

This study investigates the stabilization of self-excited rotor vibrations by active control. Rotor-dynamic systems under the influence of self-exciting mechanisms exhibit unstable behavior above some threshold speed. Quasi-linear, speed dependent models of these systems show eigenvalue excursions into the unstable zone as this threshold speed is approached. Nonlinear models with bearing deadband exhibit unstable oscillations above this same threshold speed. By the application of control forces as can be produced by magnetic bearings, the eigenvalues of the linear models are re-positioned such that the systems are stable. The control is then applied to the linear and nonlinear models by simulation. The effectiveness of the control is judged by the resulting stability characteristics of the nonlinear models and by the control bearing force levels required to maintain rotor stability.

Two rotor models are used in this study. The first of these is a two degree-of-freedom model resembling a modified Jeffcott model. Control bearing forces

1

are structured to counteract the self-exciting forces, resulting in stable operation at any rotor spin speed. By the use of a speed dependent control strategy, the eigenvalues of the closed-loop system are maintained at fixed locations. The control is chosen such that these locations match those of the original system at its optimally damped speed.

The second rotor model used in this study is a six degree-of-freedom model. It is shown to possess three natural modes, each becoming unstable at a different rotor spin speed. The stabilization of all three modes using one magnetic bearing set is investigated. The ability of the control bearing to stabilize each mode is dependent upon such factors as bearing location, feed-back signals, and control gains. The magnetic bearing location is determined by examining the uncontrolled rotor's mode shapes, with placement attempting to maxi-mize the bearing's effect on each mode. Feedback is provided through combined output signals with incomplete state information. The combination of the output sig-nals and the control gains are determined by using a search method, which maximizes the damping of the least damped mode. Control strategies using constant and speed dependent control gains are compared based upon the effect that each has on the excursions of the linear systems' eigenvalues towards the unstable zone.

CHAPTER II

BACKGROUND

The first published work dealing with the dynamics of rotating shafts was by Rankine [1] in 1869. At that time Rankine showed that rotating systems were unstable above the critical speed (the speed at which synchronous resonance occurs). Because of this, for many years manufacturers designed rotating systems to operate below the critical speed. In 1919, Jeffcott [2] identified the critical speed, not as a speed of instability, but as a natural frequency of lateral vibration. By including damping in his analysis, Jeffcott showed that stable operation was possible above the critical speed.

The increased demands on rotor systems for more power and lighter weight soon led manufacturers to design rotors for operation above the first critical speed. This led to instability problems, as rotors reached speeds above which stable operation was impossible. Several mechanisms of rotor instability have been identified and are the subject of works by Ehrich [3,4]. These include hydrodynamic bearings and seals, internal rotor friction, and turbine blade

effects. Each of the mechanisms of instability possess a common characteristic in that they produce forces tangential to radial deflections. This cross-coupling effect generally increases with speed until it overcomes the restoring and dissipative forces and the rotor becomes self-excited. Violent whirling or "whipping" of the rotor occurs as the stability threshold is reached.

While most instability mechanisms are nonlinear phenomena, they can generally be modelled as linear systems with variable coefficients. A significant non-linearity occurs, however, in bearings with radial clearances or "deadbands". Although these are not usually considered mechanisms of instability, their effect is significant on rotor performance. This effect has been examined by Childs [5] and others [6,7] whose results show that these nonlinearities often result in subsynchronous oscillations at frequencies exactly one-half of rotor spin speed. It has also been shown that bearings with radial clearances do not affect the overall stability of rotor systems.

The need for still greater performance from rotor systems requires operation at speeds above what is now the limit of stability. For this reason, the focus of much recent work has been on the improvement of rotor stability characteristics. This area has appeared more promising with the advent of active magnetic bearings.

Haberman and Liard [8] present an excellent discussion on the practical applications of these bearings. Schweitzer and Lange [9] present a more detailed description of magnetic bearing characteristics, and show how they can be implemented in a closed-loop control system. Gondhalekar and Holmes [10] discuss the various designs of magnetic bearings for controlling rotors. They show, both analytically and experimentally, how suitable configurations of magnetic bearing systems can lead to linear, uncoupled, completely determined control forces.

For stabilizing rotor systems, Burrows and Sahinkaya [11] examine the use of magnetic bearings to control oil-whirl. They apply pole-placement techniques to a single-mass, rigid rotor supported by hydrodynamic journal bearings. They determine the contol gains neccessary to position the unstable pair of eigenvalues sufficiently far from the imaginary axis, and they discuss the constraints which affect reachable pole zones. More recently, Stanway and Burrows [12] examine rotor stabilization by applying control to the rotor's support structure. They find that, with full state feedback, it is possible to obtain some degree of stabilization. They discuss the use of observers to construct the full state vector when it is not directly obtainable. Schweitzer [13] examines stabilization, using

magnetic bearings, of a linear multi-body rotor with internal damping. He uses one magnetic bearing set and defines an approach to locate the bearing based on the rotor's mode shapes. He determines an "optimal" control by maximizing the lowest damping of the system's modes. In a later work [14] he applies magnetic bearing control to a low order model obtained from a higher order modal-based model. Schweitzer then develops the control for the lower order model and examines the "spillover" effects on the higher order system.

The purpose of this study is to investigate the stabilization of self-excited rotor systems by active control. In particular, the application of linear control to nonlinear rotor systems under the influence of bearing deadband is examined. Its importance results from the fact that nearly all physical rotors supported by radial rolling element bearings are affected by deadband. While this factor is usually neglected in most rotor studies, it is one which must be understood for the full benefits of stability enhancement to be achieved.

CHAPTER III

THE TWO DEGREE-OF-FREEDOM MODEL

Introduction

The first phase of this study deals with the
stabilization of a two degree-of-freedom model which is
similar to a modified Jeffcott model. The equations of
motion for the model are developed and converted to
dimensionless form. The control strategy for rotor
stabilization is developed for the linear rotor and
applied to the linear and nonlinear models. Maximum
control bearing forces required to stabilize the rotor
are taken from dynamic simulations of linear and nonlin-
ear models. Finally, the frequency spectrum of the
nonlinear simulation is analyzed to observe the charac-
teristic behavior of the nonlinear system.

Model Development

The two degree-of-freedom model is shown in
Fig. 3.1. Although simple, this model is actually a
very useful tool in dealing with realistic rotor prob-
lems. It is widely used for conducting analytical rotor
studies, as well as gaining insight into various rotor
phenomena. More significantly, this model exhibits many

7
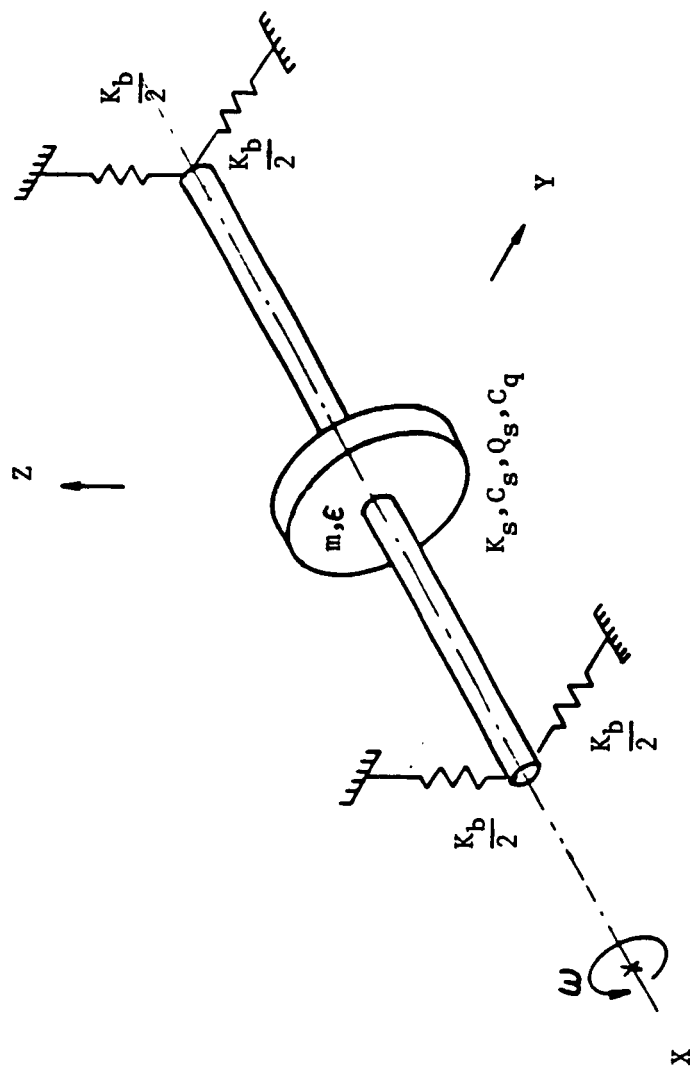
Fig. 3.1. Two Degree-of-Freedom Model.

of the types of behavior found in more complex rotor systems.

As shown in Fig. 3.1, the model consists of a uniform disk of mass m suspended by a massless rigid shaft. The bearings have a radial clearance g which provides a "deadband" in the force-deflection curve. The shaft is supported on each end by massless radial bearings having a combined linear stiffness K_b. Damping is introduced by hydrodynamic seal type elements which provide stiffness and damping K_s and C_s, respectively, and cross-coupled stiffness and damping Q_s and C_q, respectively. Although for true rotor systems most parameter values are functions of rotor spin speed, the most significant is the cross-coupled stiffness Q_s. Since this term is a source of self-excited vibration, it is sufficient to introduce speed dependency with this term only. Thus, it will be given the familiar approximate form for hydrodynamic seals,

$$Q_s = \frac{C_s \omega}{2} .$$
(3.1)

The rotor is unbalanced with the mass m at a radius ϵ. The rotor is assumed to be symmetric, both radially and laterally. The rotor spin speed ω is constant, although different speeds will be examined. Motion occurs in the Y and Z directions only.

A force diagram is shown in Fig. 3.2, where F_{bz} and F_{by} are the restoring forces from the support bearings, F_{sz} and F_{sy} are the "seal" forces, and $m\epsilon\omega^2$ is the unbalance force. Fig. 3.3 shows a force-deflection curve for the support bearings. The magnitude of the radial force produced by the bearings is given by

$$F_{br} = \begin{cases} 0 & ,|r| \leq g \\ K_b(r - g) & ,|r| > g \end{cases} \qquad (3.2)$$

with the force acting in the direction of radial displacement. Resolving this force into the Y and Z directions yields

$$F_{by} = \begin{cases} 0 & ,|r| = \sqrt{y^2 + z^2} \leq g \\ K_b(1 - \dfrac{g}{|r|})y & ,|r| > g \end{cases} \qquad (3.3)$$

and

$$F_{bz} = \begin{cases} 0 & ,|r| \leq g \\ K_b(1 - \dfrac{g}{|r|})z & ,|r| > g \end{cases} \qquad (3.4)$$

The forces due to the seals are given by

$$F_{sy} = K_s y + C_s \dot{y} + Q_s z + C_q \dot{z} \qquad (3.5)$$

and

$$F_{sz} = K_s z + C_s \dot{z} - Q_s y - C_q \dot{y}. \qquad (3.6)$$

The differing signs on the cross-coupling terms indicates a mechanism of instability.
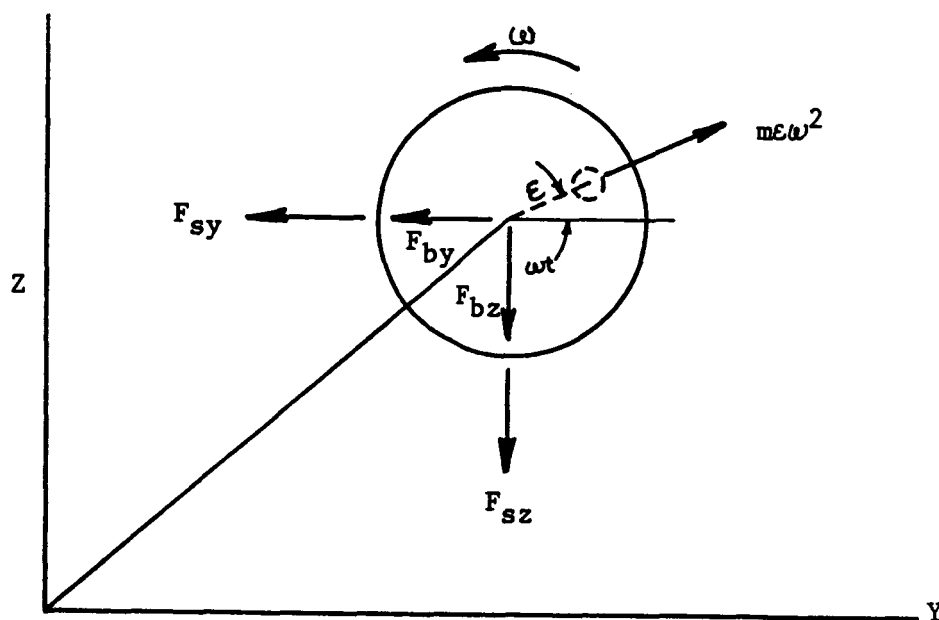
Fig. 3.2. Force Diagram for Rotor Model
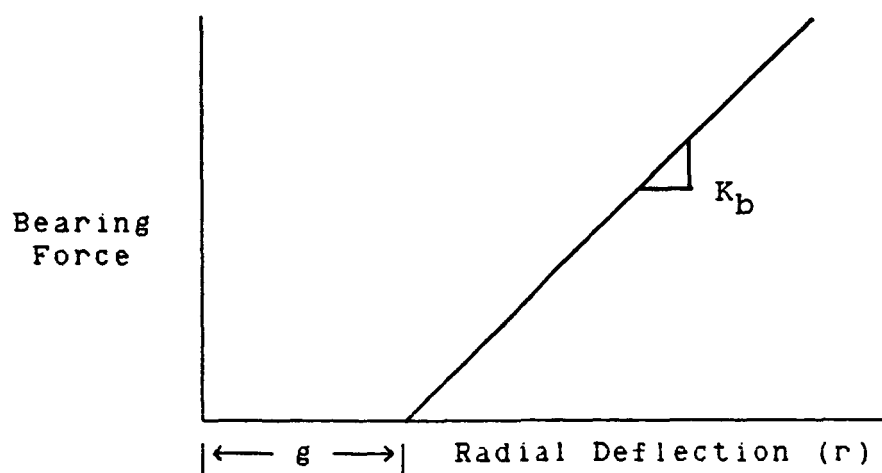
Fig. 3.3. Support Bearing Force-deflection Curve

Combining the force relationships in their respective directions yields the equations of motion for the two degree-of-freedom rotor.

$$m\ddot{y} + C_s\dot{y} + K_b(1 - \frac{g}{|r|})y + K_sy + C_q\dot{z} + Q_sz$$
$$= m\epsilon\omega^2\cos(\omega t) \qquad (3.7)$$

$$m\ddot{z} + C_s\dot{z} + K_b(1 - \frac{g}{|r|})z + K_sz - C_q\dot{y} - Q_sy$$
$$= m\epsilon\omega^2\sin(\omega t) \qquad (3.8)$$

Division by m yields

$$\ddot{y} + \frac{C_s}{m}\dot{y} + \frac{K_b}{m}(1 - \frac{g}{|r|})y + \frac{K_s}{m}y + \frac{C_q}{m}\dot{z} + \frac{Q_s}{m}z$$
$$= \epsilon\omega^2\cos(\omega t) \qquad (3.9)$$

and

$$\ddot{z} + \frac{C_s}{m}\dot{z} + \frac{K_b}{m}(1 - \frac{g}{|r|})z + \frac{K_s}{m}z - \frac{C_q}{m}\dot{y} - \frac{Q_s}{m}y$$
$$= \epsilon\omega^2\sin(\omega t) . \qquad (3.10)$$

To effect a more general study, these equations are nondimensionalized. First, a system frequency is defined as the undamped, uncoupled frequency given by

$$\omega_0^2 = \frac{K_s + K_b}{m} . \qquad (3.11)$$

By defining the dimensionless time parameter τ as

$$\tau = \omega_0 t \qquad (3.12)$$

and using the chain rule it follows that

$$\dot{y} = \frac{dy}{dt} = \frac{dy}{d\tau}\frac{d\tau}{dt} = \omega_0 \frac{dy}{dt} = \omega_0 y'. \qquad (3.13)$$

Similarly,

$$\ddot{y} = \zeta_0^2 y'', \qquad (3.14)$$

$$\dot{z} = \omega_0 z', \qquad (3.15)$$

and

$$\ddot{z} = \zeta_0^2 z''. \qquad (3.16)$$

Substituting for t, using (3.13) - (3.16) and dividing by ω_0^2 yields

$$y'' + \frac{C_s}{m\omega_0} y' + \frac{K_b}{m\omega_0^2}(1 - \frac{g}{|r|})y + \frac{K_s}{m\omega_0^2} y + \frac{C_q}{m\omega_0} z'$$

$$+ \frac{Q_s}{m\omega_0^2} z = \frac{\omega^2}{\omega_0^2}\cos\left(\frac{\omega}{\omega_0}\tau\right). \qquad (3.17)$$

and

$$z'' + \frac{C_s}{m\omega_0} z' + \frac{\bar{K}_b}{m\omega_0{}^2}\left(1 - \frac{g}{|r|}\right)z + \frac{K_s}{m\omega_0{}^2} z - \frac{C_q}{m\omega_0} y'$$

$$- \frac{Q_s}{m\omega_0{}^2} y = \frac{\omega^2}{\omega_0{}^2}\sin\left(\frac{\omega}{\omega_0}\tau\right). \qquad (3.18)$$

Now make the following definitions:

$$\frac{\omega}{\omega_0} = R, \qquad \zeta_s = \frac{C_s}{2m\omega_0}, \qquad \zeta_q = \frac{C_q}{2m\omega_0},$$

$$R_{Kb} = \frac{K_b}{K_s + K_b} = \frac{K_b}{m\omega_0{}^2}, \qquad R_{Ks} = \frac{K_s}{K_s + K_b} = \frac{K_s}{m\omega_0{}^2},$$

$$Q_s = \frac{C_s\omega}{2}, \quad \text{so} \quad \frac{Q_s}{m\omega_0{}^2} = \frac{C_s}{2m\omega_0}\frac{\omega}{\omega_0} = \zeta_s R.$$

Substituting these yields

$$y'' + 2\zeta_s y' + R_{Kb}\left(1 - \frac{g}{|r|}\right)y + R_{Ks}y + 2\zeta_q z'$$

$$+ \zeta_s R z = R^2 \epsilon \cos(R\tau) \qquad (3.19)$$

and

$$z'' + 2\zeta_s z' + R_{Kb}\left(1 - \frac{g}{|r|}\right)z + R_{Ks}z - 2\zeta_q y'$$

$$- \zeta_s R y = R^2 \epsilon \sin(R\tau). \qquad (3.20)$$

Finally, division by a characteristic length, say ϵ, yields the dimensionless model

$$\bar{y}'' + 2\zeta_s\bar{y}' + R_{kb}(1 - \frac{\bar{g}}{|\bar{r}|})\bar{y} + R_{ks}\bar{y} + 2\zeta_q\bar{z}'$$

$$+ \zeta_sR\bar{z} = R^2\cos(R\tau) \qquad (3.21)$$

and

$$\bar{z}'' + 2\zeta_s\bar{z}' + R_{kb}(1 - \frac{\bar{g}}{|\bar{r}|})\bar{z} + R_{ks}\bar{z} - 2\zeta_q\bar{y}'$$

$$- \zeta_sR\bar{y} = R^2\sin(R\tau). \qquad (3.22)$$

Table 3.1 summarizes the dimensionless parameter definitions.

Equations (3.21) and (3.22) represent the non-linear, uncontrolled rotor. Defining the state vector $\underline{x}$ as

$$\underline{x} = [\bar{y} \; \bar{z} \; \bar{v}_y \; \bar{v}_z]^T \qquad (3.23)$$

the system in first-order form becomes

$$\underline{x}' = A\underline{x} + \underline{d} \qquad (3.24)$$

where

$$A = \begin{bmatrix} 0 & 0 & 1 & 0 \\ 0 & 0 & 0 & 1 \\ -(R_{ks} + R_{kb}) & -\zeta_sR & -2\zeta_s & -2\zeta_q \\ \zeta_sR & -(R_{ks} + R_{kb}) & 2\zeta_q & -2\zeta_s \end{bmatrix} \qquad (3.25)$$

and

$$
\underline{d} = \begin{bmatrix} 0 \\ 0 \\ R^2\cos(R\tau) + R_{kb}\left(\dfrac{\bar{g}}{|\bar{r}|}\right)\bar{y} \\ R^2\sin(R\tau) + R_{kb}\left(\dfrac{\bar{g}}{|\bar{r}|}\right)\bar{z} \end{bmatrix} . \tag{3.26}
$$

Note that the vector $\underline{d}$ contains both the unbalance forces and the nonlinear contributions from the support bearings. The same restrictions apply as in equations (3.3) and (3.4) to the nonlinear terms, i.e.,

$$
R_{kb}\left(1 - \frac{\bar{g}}{|\bar{r}|}\right) = 0, \quad \text{if} \quad |\bar{r}| \leq \bar{g} .
$$

Also note that, by definition, $R_{ks} + R_{kb} = 1$, so the system matrix becomes

$$
A = \begin{bmatrix} 0 & 0 & 1 & 0 \\ 0 & 0 & 0 & 1 \\ -1 & -\zeta_s R & -2\zeta_s & -2\zeta_q \\ \zeta_s R & -1 & 2\zeta_q & -2\zeta_s \end{bmatrix} . \tag{3.27}
$$

Table 3.1

Dimensionless Parameter Definitions

Nomenclature	Parameter	Equivalent
Frequency	ω_o	$\sqrt{\dfrac{K_s + K_b}{m}}$
Damping	ζ_s	$\dfrac{C_s}{2m\omega_o}$
Stiffness	R_{kb}	$\dfrac{K_b}{K_s + K_b}$
	R_{ks}	$\dfrac{K_s}{K_s + K_b}$
Cross-Coupled Damping	ζ_q	$\dfrac{C_q}{2m\omega_o}$
Cross-Coupled Stiffness	$\zeta_s R$	$\zeta_s R$
Spin Speed	R	$\dfrac{\omega}{\omega_o}$
Displacements	$\bar{y}$	$\dfrac{y}{\epsilon}$
	$\bar{z}$	$\dfrac{z}{\epsilon}$
Deadband	$\bar{g}$	$\dfrac{g}{\epsilon}$
Time	τ	$\omega_o t$

Characteristics of the Uncontrolled Rotor

This study concerns stabilization of rotors for speeds at which the uncontrolled rotor is unstable. For nonlinear systems, however, stability and instability are amplitude dependent. When examining the instability of a rotor with deadband, it is apparent that the effect of the deadband is diminished as the rotor's amplitudes of vibration begin to grow. Global stability can be determined by neglecting the deadband, producing a linear system compatible with various linear analysis techniques. Therefore, this study deals with analyzing linear systems obtained by neglecting deadband. The results of these analyses are applied to the nonlinear system, which is examined by simulation.

The eigenvalues of the linear system can be readily obtained and will provide nearly all of the information required, both for examining the stability of the rotor and for determining the desired control laws. Examination of the system matrix A shows a speed dependency in the term $\zeta_s R$. Thus, for any given speed R, a different linear system is obtained. At some speed, the system becomes unstable. That speed is the onset speed of instability or the instability threshold speed. Using the parameter values shown in Table 3.2, the system eigenvalues over the speed range $0 \leq R \leq 5$

are shown in Fig. 3.4. The system is at the threshold
of instability for a speed of R = 2.2. The frequency of
the unstable mode ("whirl") is 1.1, approximately one-
half that of the rotor spin speed, characteristic of
self-excited rotors. As expected, the nonlinear system
with deadband becomes unstable above R = 2.2. This is
shown by simulation results depicted in Fig. 3.5, using
a deadband $\bar{g}$ = 1 for R = 2.3.

Table 3.2

System Parameter Values

Parameter	Value
ζ_s	0.5
ζ_q	0.1
R_{kb}	0.8
R_{ks}	0.2

UNCONTROLLED ROTOR POLES

(0 < R < 5)

Real Axis

Imaginary Axis

R=2.2

Fig. 3.4. Uncontrolled Rotor Pole Trace.

ROTOR CENTER POSITION

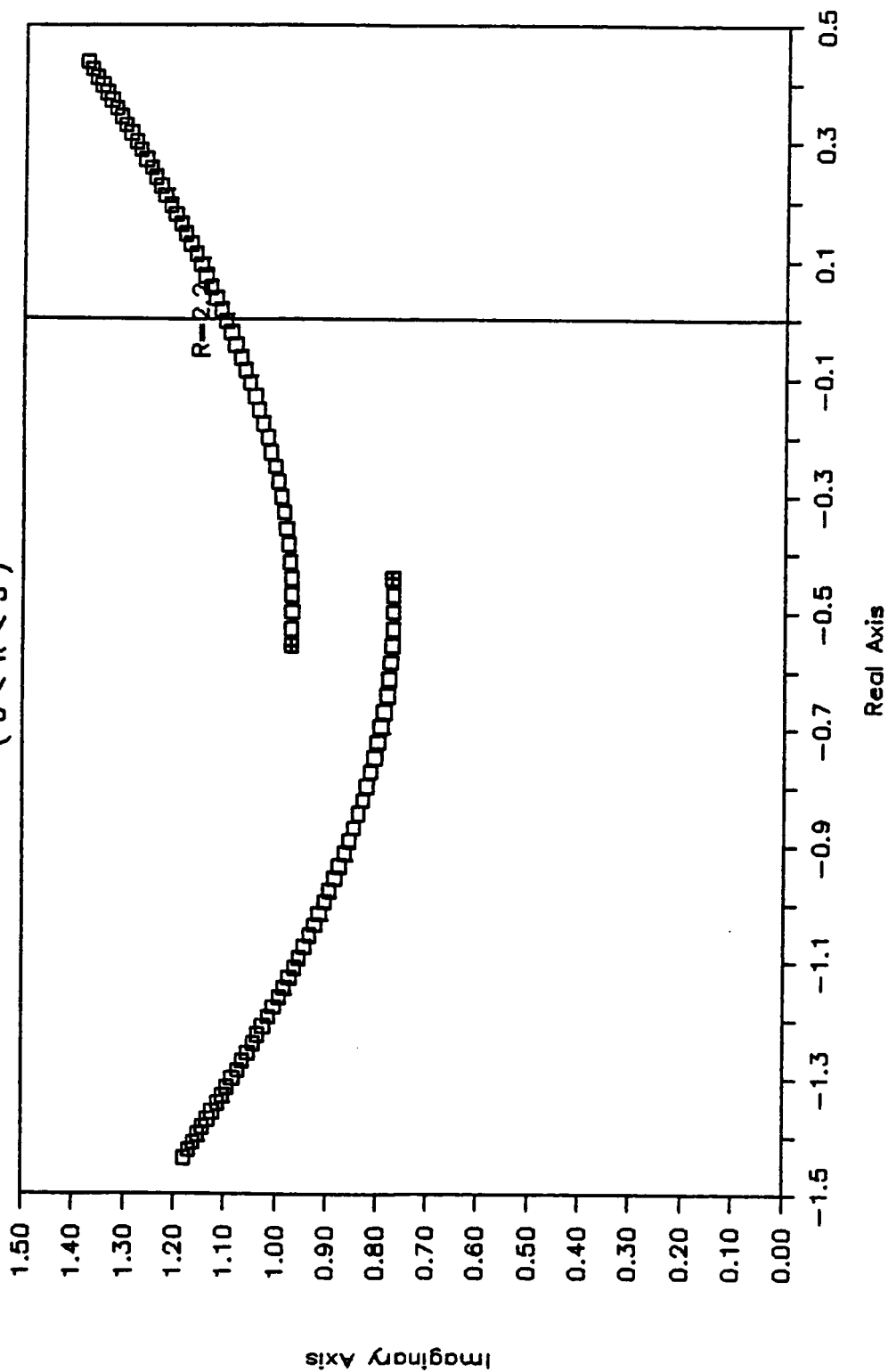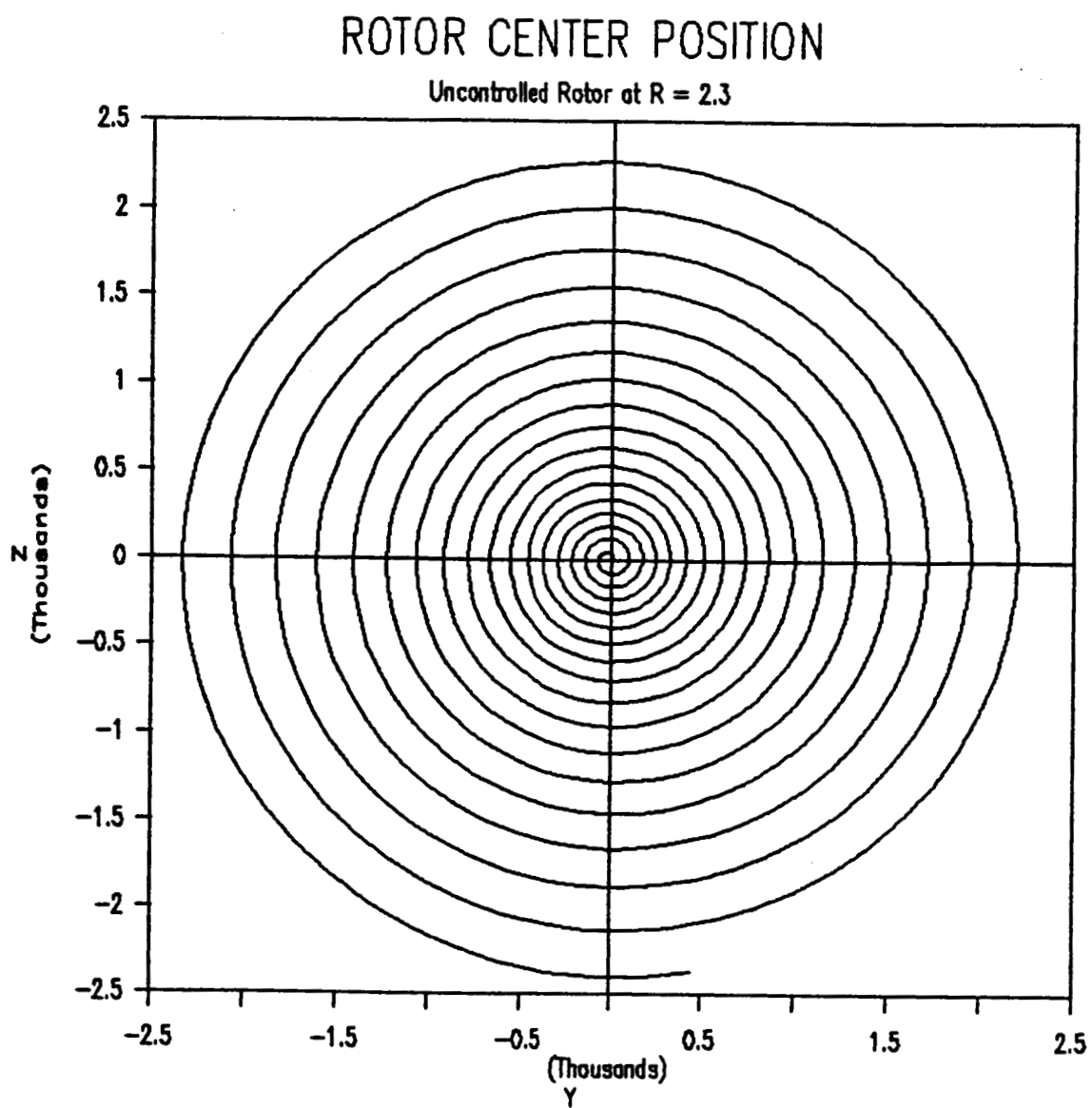## Uncontrolled Rotor at R = 2.3

Fig. 3.5. Unstable Response of Nonlinear System at R = 2.3.

The Control Actuator

The problems of applying completely definable forces to high speed rotating machinery have been the focus of much recent study [8, 9, 10]. The result of this effort is a versatile class of devices widely known as magnetic bearings. These bearings utilize electromagnetic interaction to produce forces on shafts suspended within their housings. Many experimental studies and several practical applications attest to the feasibility of these bearings for use in rotating machinery.

The force produced by a magnetic bearing can be made relatively proportional to the driving current. The use of two bearings grouped together results in a device which can produce two independent forces in arbitrary directions. By structuring the input currents to be functions of the states of the system, a closed-loop control system is produced. The forces can be made to resemble stiffness, damping, combinations of these, or other suitable forms.

For the purposes of this study, the magnetic bearing forces are assumed to act in orthogonal directions coinciding with the Y and Z rotor coordinate directions. The transients associated with the actuator and control loop are assumed to be negligible compared with those of the rotor. The input current is proportioned to the state vector $\underline{x}$ through a gain matrix G so that

$$\underline{u} = \begin{bmatrix} u_1 \\ u_2 \end{bmatrix} = -G\underline{x} \qquad (3.28)$$

where

$$G = \begin{bmatrix} g_{11} & g_{12} & g_{13} & g_{14} \\ g_{21} & g_{22} & g_{23} & g_{24} \end{bmatrix}. \qquad (3.29)$$

Stabilizing the Rotor

Modifying equation (3.24) to include the control forces acting through a control distribution matrix B yields

$$\underline{x}' = A\underline{x} + B\underline{u} + \underline{d}. \qquad (3.30)$$

Again, since system stability is of interest, bearing deadband is temporarily neglected. The stability of linear systems is independent of input, so the vector $\underline{d}$ is neglected temporarily as well. The resulting linear system is

$$\underline{x}' = A\underline{x} + B\underline{u} \qquad (3.31)$$

or

$$\underline{x}' = (A - BG)\underline{x}. \qquad (3.32)$$

Since there are independent, unconstrained control forces acting in each direction, it can be shown that all states are accessible by the control, and the system is controllable. Thus, by selection of the gain matrix G, the eigenvalues of (A - BG) can be arbitrarily positioned.

A simple method for stabilizing the rotor can be developed by examination of the closed-loop system matrix (A - BG). From the definition of the state vector $\underline{x}$ and the form of the input $\underline{u}$, the control distribution matrix B has the form

$$B = \begin{bmatrix} 0 \\ - - - \\ I \end{bmatrix}. \tag{3.33}$$

This results in the closed-loop system matrix

$$(A - BG) = \begin{bmatrix} 0 & 0 & 1 & 0 \\ 0 & 0 & 0 & 1 \\ -(1+g_{11}) & -(\zeta_s R+g_{12}) & -(2\zeta_s+g_{13}) & -(2\zeta_q+g_{14}) \\ (\zeta_s R-g_{21}) & -(1+g_{22}) & (2\zeta_q-g_{23}) & -(2\zeta_s+g_{24}) \end{bmatrix}. \tag{3.34}$$

Since the rotor is radially symmetric, it follows that the control should conform to the same symmetry.

Therefore

$$g_{21} = -g_{12} \tag{3.35}$$

$$g_{22} = g_{21} \tag{3.36}$$

$$g_{23} = -g_{14} \tag{3.37}$$

and

$$g_{24} = g_{13} . \tag{3.38}$$

Thus,

$$(A - BG) = \begin{bmatrix} 0 & 0 & 1 & 0 \\ 0 & 0 & 0 & 1 \\ -(1+g_{11}) & -(\zeta_s R + g_{12}) & -(2\zeta_s + g_{13}) & -(2\zeta_q + g_{14}) \\ (\zeta_s R + g_{12}) & -(1+g_{11}) & (2\zeta_q + g_{14}) & -(2\zeta_s + g_{13}) \end{bmatrix} .$$

$$\tag{3.39}$$

Examination of this matrix shows a speed dependency only with the term $(\zeta_s R + g_{12})$. By selection of g_{12} as a linear function of R, this term can be held constant for any spin speed. Furthermore, by setting $g_{11} = g_{13} = g_{14} = 0$, the above matrix at an arbitrary spin speed can be made equal to the open-loop matrix A at some speed, say R_0. In other words, making

$$g_{12} = \zeta_s (R_0 - R) \tag{3.40}$$

will make

$$(A - BG)_R = A_{R_O} .$$ (3.41)

This essentially cancels the effect of the cross-coupled stiffness, which is the mechanism of instability in this model. Furthermore, the eigenvalues of (A - BG) at any spin speed R remain constant and equal to those of A at the speed R_O. Thus, the problem of control determination is reduced to choosing the speed R_O for which the system has the desired characteristics.

One logical choice of the "reference speed" R_O can be made by examining the pole-trace of Fig. 3.4. At the speed R = 0, the system has the highest relative damping of any speed. Relative damping associated with the ith mode is defined as

$$\zeta_{RD} = \frac{-\delta_i}{\sqrt{\delta_i^2 + \omega_i^2}}$$ (3.42)

where $\lambda_i = \delta_i \pm j\omega_i$ represents the ith eigenvalue of the system. As an eigenvalue moves towards the unstable zone, its relative damping decreases. The minimum relative damping thus becomes a useful measure of the stability of the system. At R = 0, this value is maximum ($\zeta_{RD} = 0.497$), with both modes being equally damped. For comparison, the minimum relative damping at the uncontrolled first critical speed of R = 0.78 is $\zeta_{RD} = 0.323$. Thus, the choice of $R_O = 0$ results in an

"optimally" stable system with a 54% increase in critical speed damping. ("Optimal" of course, refers only to the control approach chosen here.)

Using equation (3.40) with $R_0 = 0$ yields

$$g_{12} = -\zeta_s R \qquad\qquad (3.43)$$

and

$$G = \begin{bmatrix} 0 & -\zeta_s R & 0 & 0 \\ \zeta_s R & 0 & 0 & 0 \end{bmatrix} . \qquad\qquad (3.44)$$

This keeps the poles of the closed-loop system at

$$\lambda_1 = -0.55723 \pm j(0.97366), \text{ and}$$

$$\lambda_2 = -0.44272 \pm j(0.77366)$$

for any rotor spin speed R.

Control Performance

While knowledge of the system poles gives an indication of the degree of stability and damping of the system, it gives no insight into other factors relative to the performance of the control. For example, while the implemented gains may cause a stable eigenvalue assignment, the force levels required to accomplish the stabilization may be higher than the physical actuators can produce. Also, the control of the nonlinear system

is of concern. These questions can be addressed by dynamically simulating the controlled rotor.

Using the control developed in the previous section, numerous simulations were conducted for various spin speeds and bearing deadband values. Fig. 3.6 shows a typical simulation result. For each case, the maximum control force required during the steady-state rotor response was computed. These are plotted in Fig. 3.7 versus spin speed. The three cases include the linear system ($\bar{g} = 0$) and two nonlinear systems ($\bar{g} = 1$, and $\bar{g} = 10$). This figure shows a nearly linear dependence of the maximum control force on the spin speed R. Furthermore, the variation between linear and nonlinear cases is slight, if not negligible. Another interesting performance indicator is how well the rotor responds to an impulsive disturbance. Fig. 3.8 through Fig. 3.10 show the rotor response to an impulse velocity in one direction. Again, the cases include the linear system and two nonlinear systems, showing the maximum control force for each. While for these cases the maximum forces are higher and increase with deadband, this is to be expected. Loss of stiffness due to deadband causes a greater excursion from the steady-state orbit, producing a higher control force.

Finally, the frequencies of a rotor orbit are often of interest. Sub-synchronous whirls cause cyclic

flexure of the rotor shaft and are often destructive.
They also indicate the presence of self-excited vibra-
tion mechanisms which lead to instability as the speed
is increased. Fig. 3.11 shows the frequency composition
of the rotor response of Fig. 3.10. it is predominantly
synchronous, as the self-exciting forces are counter-
acted by the control, and subsynchronous components are
not detectable.

Summary

In this chapter, a two degree-of freedom model was
developed and stabilized for an arbitrary speed . While
the control approach utilized was fairly simplistic, it
was shown to be quite effective. More importantly, it
allowed for an evaluation of the control performance.
While such indicators as control force levels and the
response of the nonlinear rotor may change quantita-
tively for different control schemes, the trend of each
would probably not differ substantially. The results of
this chapter will be applied to a more realistic, com-
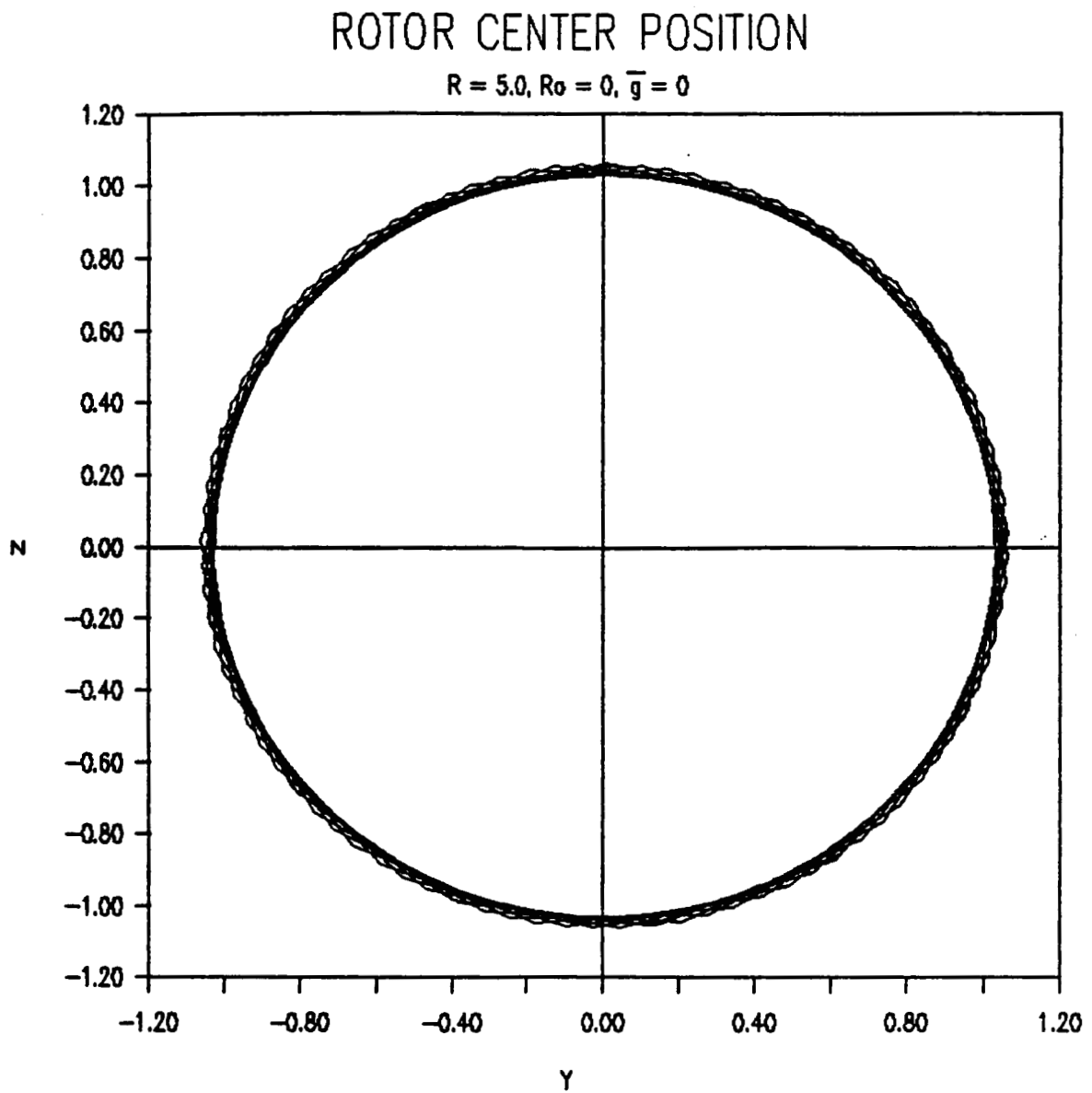plex rotor system in chapter four.

ROTOR CENTER POSITION

$R = 5.0$, $Ro = 0$, $\overline{g} = 0$

Fig. 3.6.   Rotor Response at $R = 5$, $\overline{g} = 0$.

MAXIMUM CONTROL FORCE Vs SPIN SPEED

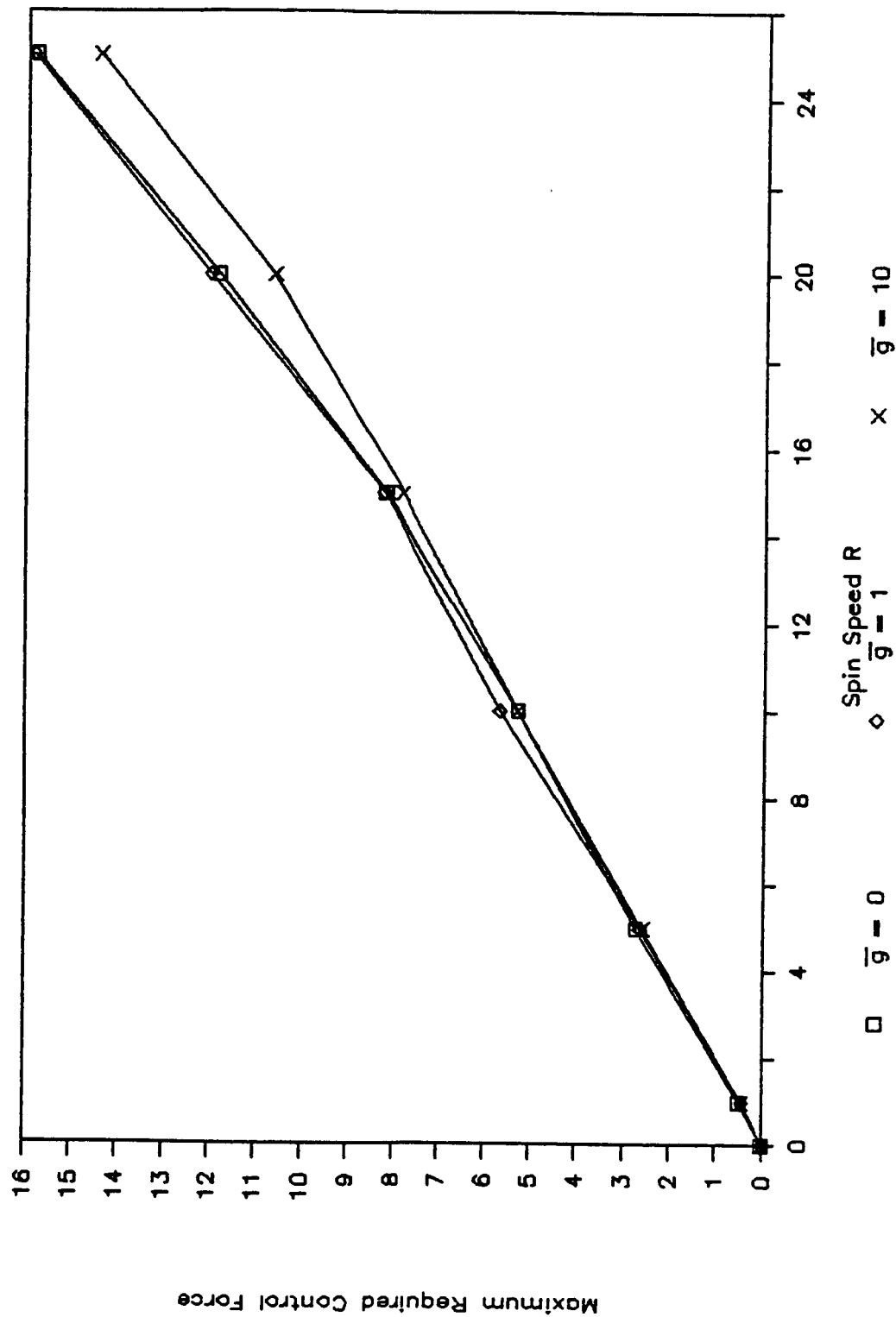Fig. 3.7. Maximum Required Control Force Vs. Spin Speed.

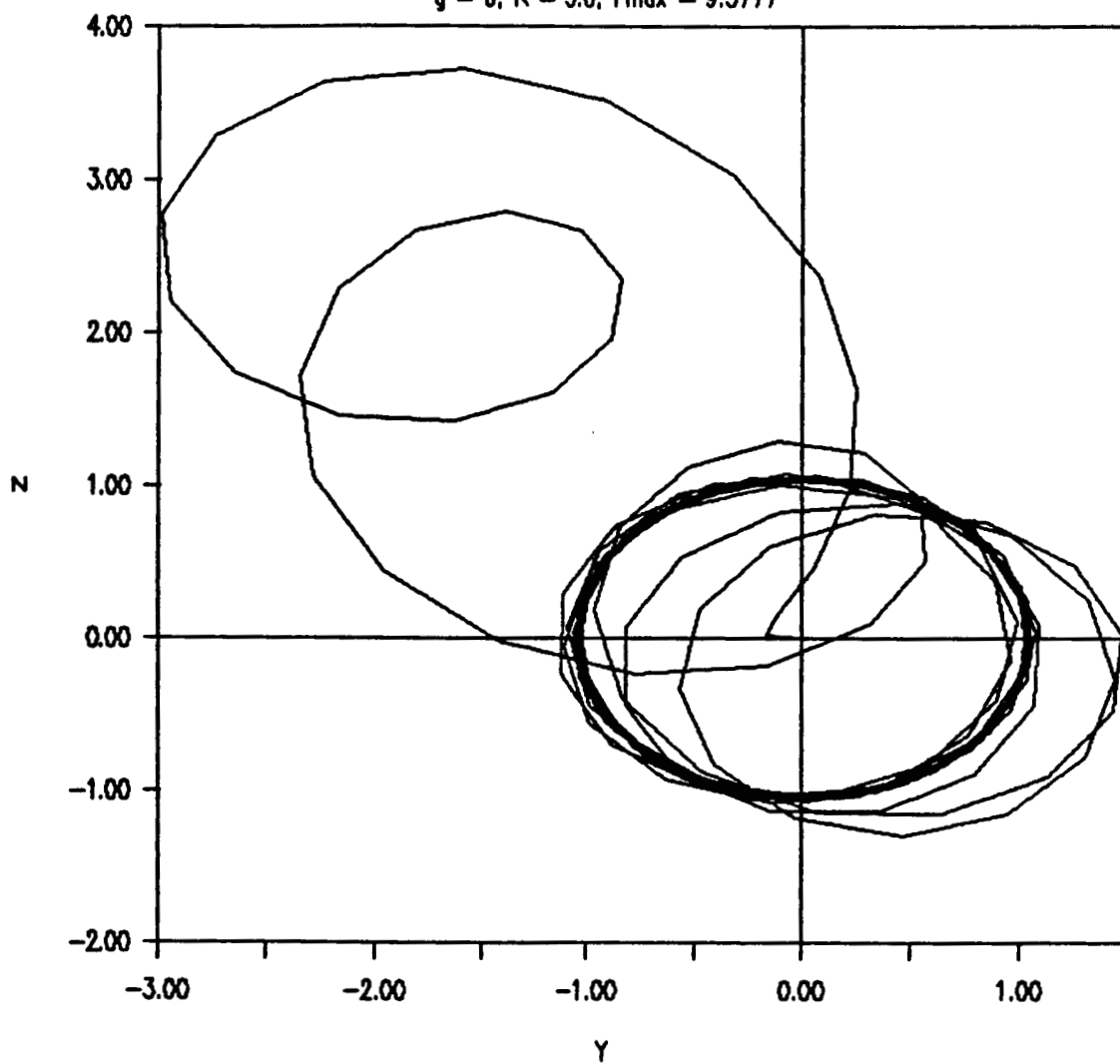ROTOR RESPONSE TO IMPULSE

$\bar{g} = 0$, R = 5.0, Fmax = 9.3777

Fig. 3.8.   Rotor Response to Impulse at R = 5, $\bar{g}$ = 0.

ROTOR RESPONSE TO IMPULSE
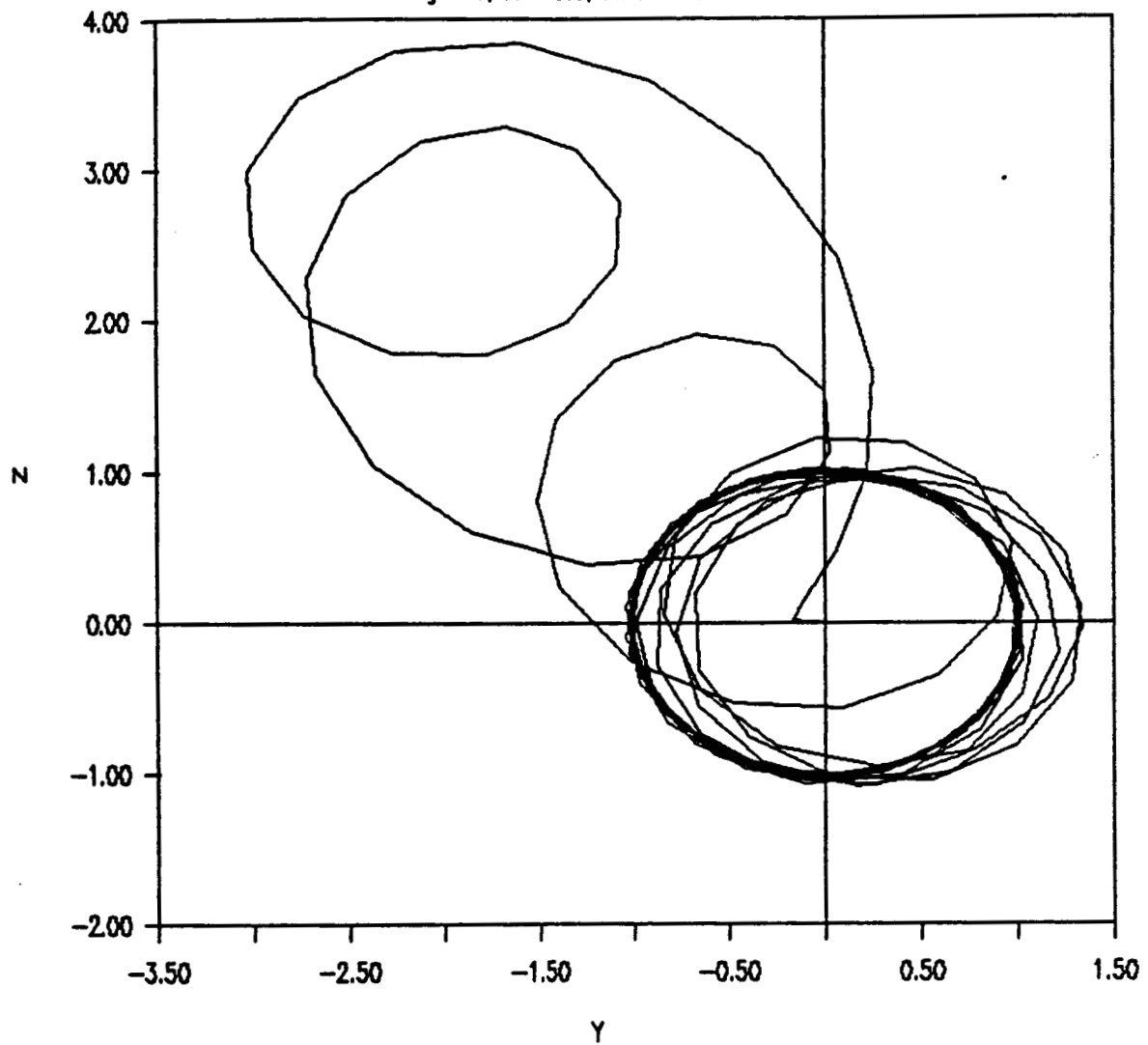
$\bar{g} = 1$, R = 5.0, Fmax = 9.7128

Fig. 3.9.   Rotor Response to Impulse at R = 5, $\bar{g}$ = 1.

ROTOR RESPONSE TO IMPULSE

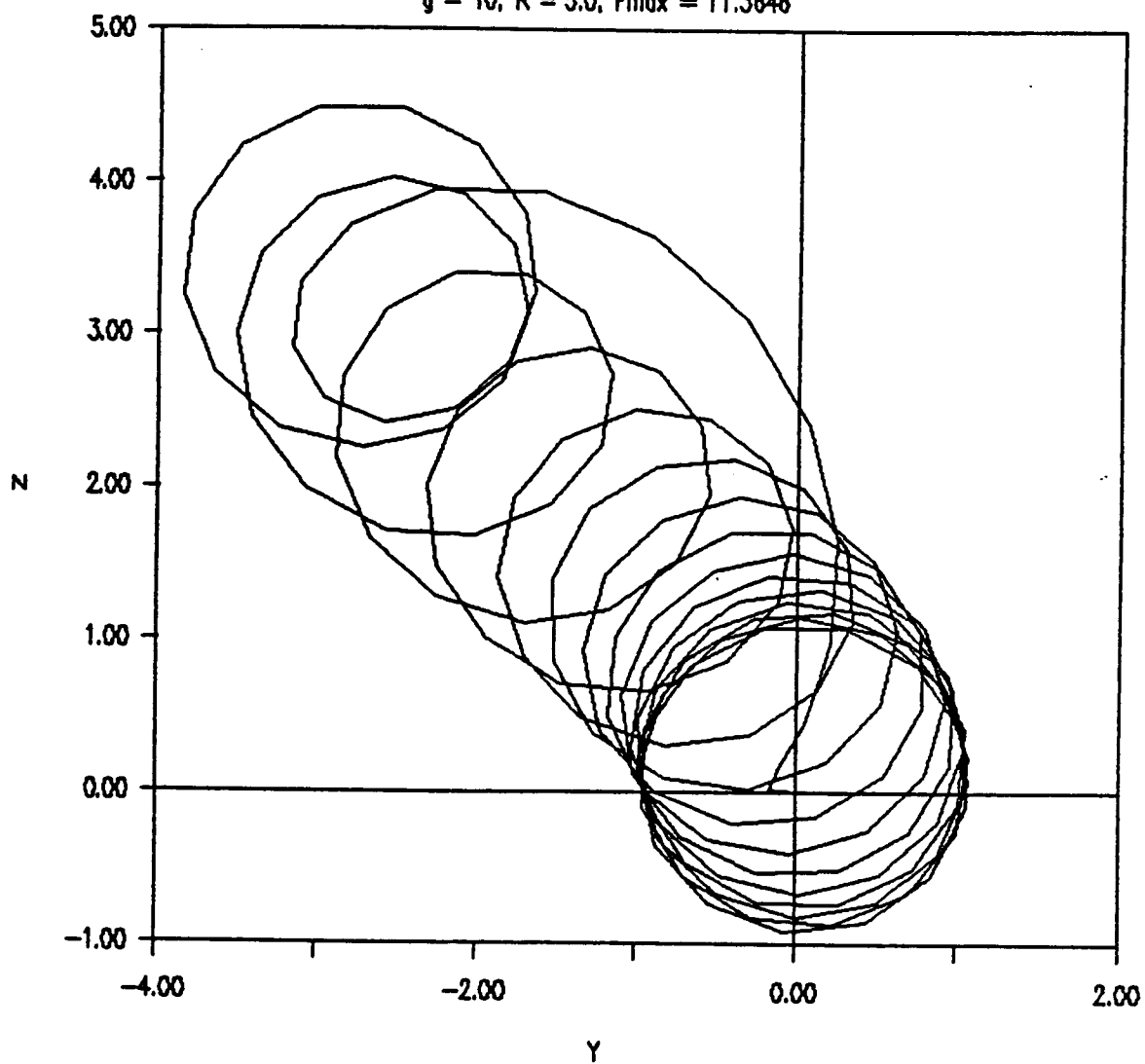$\bar{g} = 10$, R = 5.0, Fmax = 11.3646

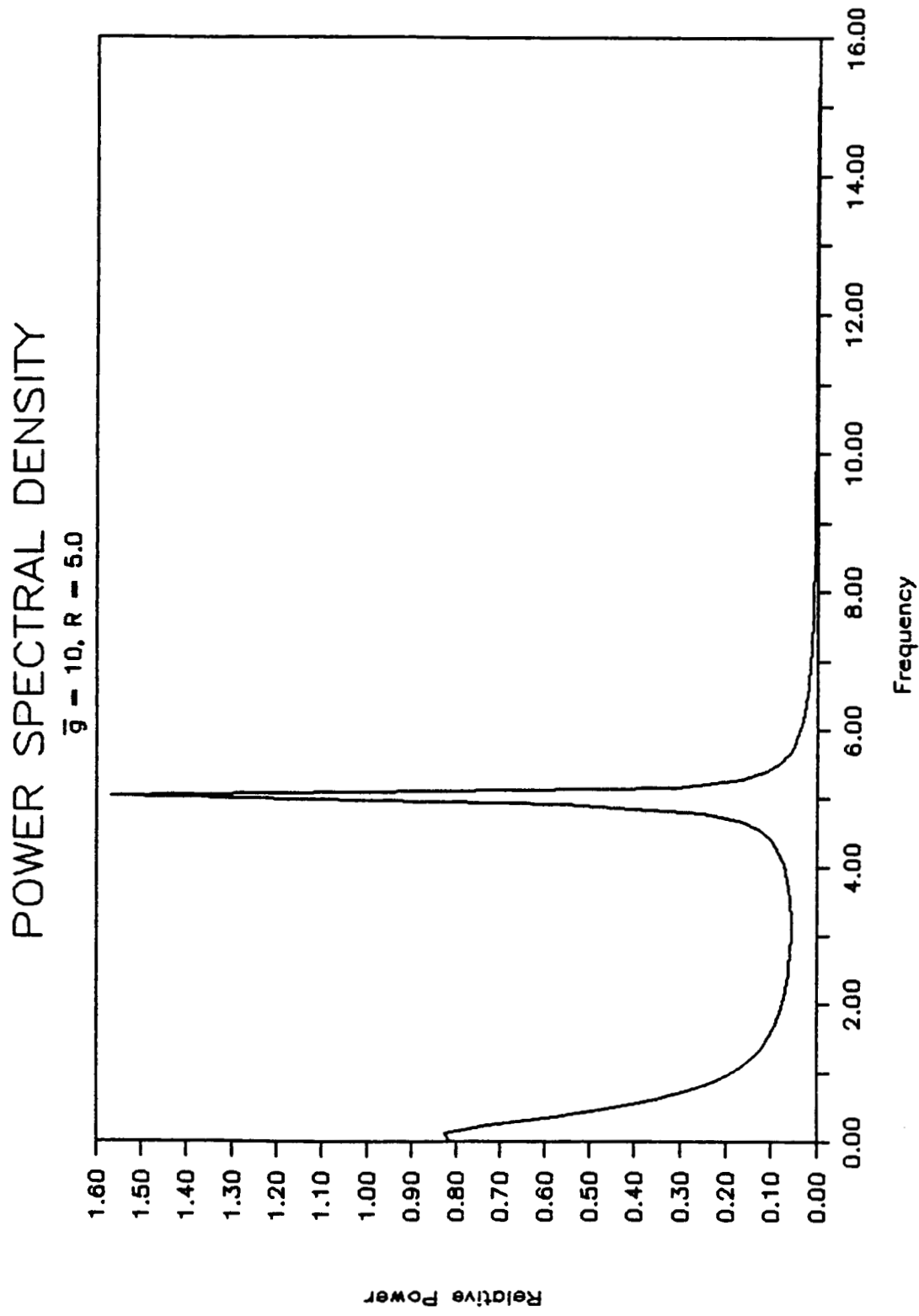Fig. 3.10. Rotor Response to Impulse at R = 5, $\bar{g}$ = 10.

POWER SPECTRAL DENSITY

$\bar{g} = 10$, R = 5.0

Relative Power

Frequency

Fig. 3.11. Power Spectral Density for Response of Fig. 3.10.

CHAPTER IV

THE SIX DEGREE-OF-FREEDOM MODEL

Introduction

This chapter deals with stabilizing a six degree-of-freedom rotor using one active magnetic bearing set. In the previous chapter, a two degree-of-freedom rotor was stabilized by using the control bearing to counteract self-exciting forces. The result was a rotor that was stable for any given spin speed. In many physical rotors, however, the locations of self-exciting mechanisms dimensionally restrict the positioning and number of control forces that may be applied. Full state feedback for large rotor systems would also be impractical. For these reasons, the six degree-of-freedom rotor model is examined. This model enables the introduction of several self-exciting mechanisms and nonlinearities located away from the point of control application. To investigate the stabilization of this rotor, the model is presented in dimensionless form. Its uncontrolled characteristics are studied to determine such factors as control location and signal measurement. An "optimal" stability criterion is defined using the eigenvalues of

36

the linear system. The control gains are determined by
a search method. Finally, simulations are conducted to
determine required control force levels for the linear
and nonlinear systems.

The Model

The six degree-of-freedom model is shown in
Fig. 4.1. This rotor has three uniform lumped masses
m_1, m_2, and m_3 connected by two massless, flexible
shafts of stiffness K_{f1} and K_{f2}. Acting at each mass
are support bearings K_1, K_2 and K_3, respectively. These
are radial type bearings, each with a deadband g_i,
(i = 1, 2, 3). Also at each mass are elements which pro-
vide cross-coupled stiffness and damping Q_{si} and C_{qi},
as well as support stiffness and damping K_{si} and C_{si}.
Each mass is "unbalanced" by its mass m_i at a radius ϵ_i,
where all three unbalanced radii are assumed to lie in
the same plane. The rotor is assumed to be radially
symmetric operating at a constant spin speed ω. Only
motion in the Y and Z directions is considered. Gyro-
scopic effects, which can be shown to enhance rotor sta-
bility, are neglected.

The support bearings are initially assumed to have
zero deadband. This simplifies the form of the equa-
tions of motion. The nonlinear contributions from dead-
band are included during the simulations by a

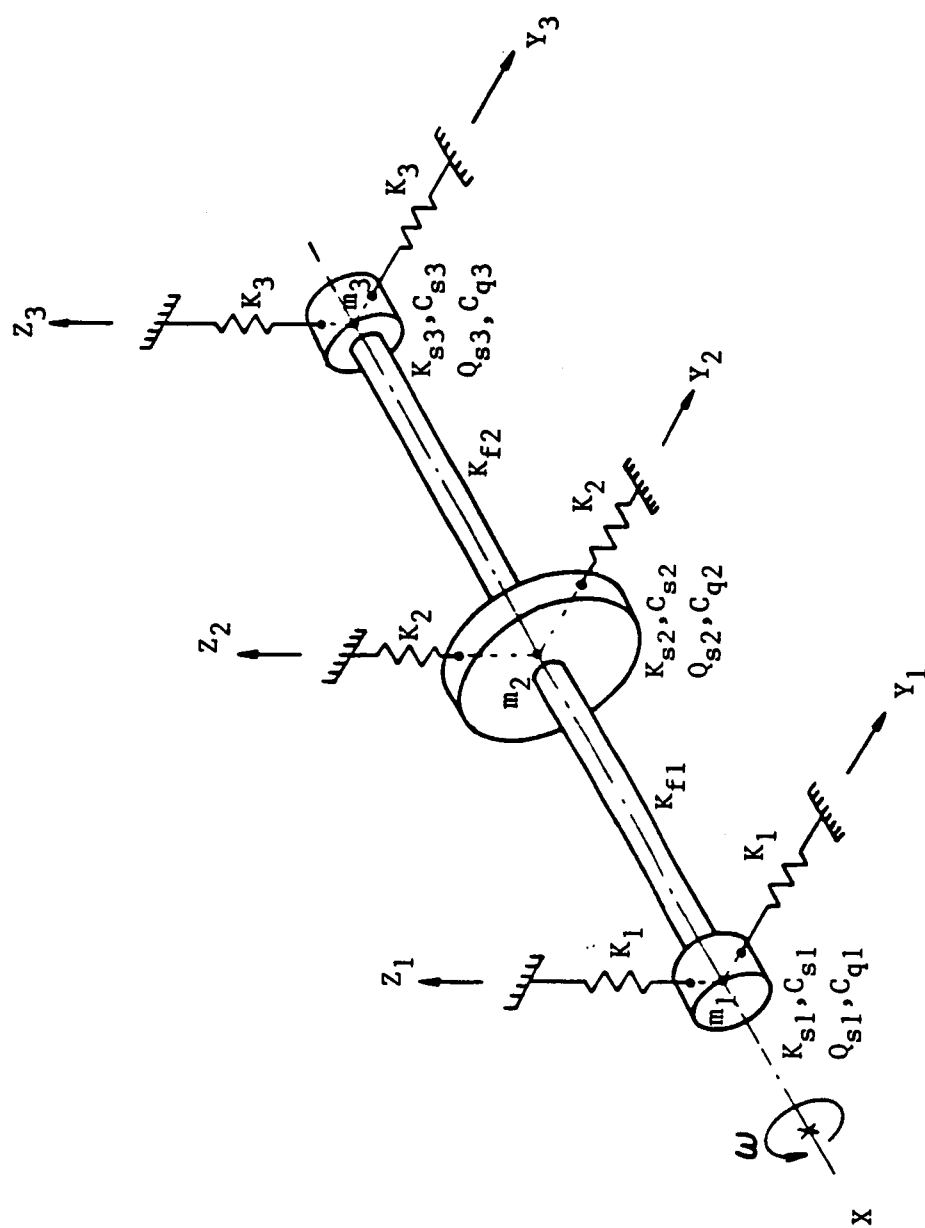Fig. 4.1. Six Degree-of-Freedom Model.

disturbance vector. The resulting system is linear with the following equations of motion:

$$m_1\ddot{y}_1 + C_1\dot{y}_1 + (K_{s1} + K_1)y_1 + K_{f1}(y_1 - y_2)$$
$$+ C_{q1}\dot{z}_1 + Q_{s1}z_1 = m_1\omega^2\epsilon_1\cos(\omega t) \qquad (4.1)$$

$$m_1\ddot{z}_1 + C_1\dot{z}_1 + (K_{s1} + K_1)z_1 + K_{f1}(z_1 - z_2)$$
$$- C_{q1}\dot{y}_1 - Q_{s1}y_1 = m_1\omega^2\epsilon_1\sin(\omega t) \qquad (4.2)$$

$$m_2\ddot{y}_2 + C_2\dot{y}_2 + (K_{s2} + K_2)y_2 + K_{f1}(y_2 - y_1)$$
$$+ K_{f2}(y_2 - y_3) + C_{q2}\dot{z}_2 + Q_{s2}z_2 = m_2\omega^2\epsilon_2\cos(\omega t) \qquad (4.3)$$

$$m_2\ddot{z}_2 + C_2\dot{z}_2 + (K_{s2} + K_2)z_2 + K_{f1}(z_2 - z_1)$$
$$+ K_{f2}(z_2 - z_3) - C_{q2}\dot{y}_2 - Q_{s2}y_2 = m_2\omega^2\epsilon_2\sin(\omega t) \qquad (4.4)$$

$$m_3\ddot{y}_3 + C_3\dot{y}_3 + (K_{s3} + K_3)y_3 + K_{f2}(y_3 - y_2)$$
$$+ C_{q3}\dot{z}_3 + Q_{s3}z_3 = m_3\omega 2\epsilon_3\cos(\omega t) \qquad (4.5)$$

$$m_3\ddot{z}_3 + C_3\dot{z}_3 + (K_{s3} + K_3)z_3 + K_{f2}(z_3 - z_2)$$
$$- C_{q3}\dot{y}_3 - Q_{s3}y_3 = m_3\omega^2\epsilon_3\sin(\omega t) \qquad (4.6)$$

By defining the dimensionless parameters shown in Table 4.1, the equations are nondimensionalized and become:

$$\bar{y}_1{''} + 2\zeta_1\bar{y}_1{'} + \frac{R_{k1}}{R_{m1}}\bar{y}_1 + \frac{R_{f1}}{R_{m1}}(\bar{y}_1 - \bar{y}_2)$$
$$+ 2\zeta_{q1}\bar{z}_1{'} + \frac{\zeta_1 R}{R_{m1}}\bar{z}_1 = R_{\epsilon1}R^2\cos(R\tau) \qquad (4.7)$$

$$\bar{z}_1'' + 2\zeta_1\bar{z}_1' + \frac{R_{k1}}{R_{m1}}\bar{z}_1 + \frac{R_{f1}}{R_{m1}}(\bar{z}_1 - \bar{z}_2)$$

$$- 2\zeta_{q1}\bar{y}_1' - \frac{\zeta_1 R}{R_{m1}}\bar{y}_1 = R_{\epsilon1}R^2\sin(R\tau) \qquad (4.8)$$

$$\bar{y}_2'' + 2\zeta_2\bar{y}_2' + \frac{R_{k2}}{R_{m2}}\bar{y}_2 + \frac{R_{f1}}{R_{m2}}(\bar{y}_2 - \bar{y}_1) + \frac{R_{f2}}{R_{m2}}(\bar{y}_2 - \bar{y}_3)$$

$$+ 2\zeta_{q2}\bar{z}_2' + \frac{\zeta_2 R}{R_{m2}}\bar{z}_2 = R_{\epsilon2}R^2\cos(R\tau) \qquad (4.9)$$

$$\bar{z}_2'' + 2\zeta_2\bar{z}_2' + \frac{R_{k2}}{R_{m2}}\bar{z}_2 + \frac{R_{f1}}{R_{m2}}(\bar{z}_2 - \bar{z}_1) + \frac{R_{f2}}{R_{m2}}(\bar{z}_2 - \bar{z}_3)$$

$$- 2\zeta_{q2}\bar{y}_2' - \frac{\zeta_2 R}{R_{m2}}\bar{y}_2 = R_{\epsilon2}R^2\sin(R\tau) \qquad (4.10)$$

$$\bar{y}_3'' + 2\zeta_3\bar{y}_3' + \frac{R_{k3}}{R_{m3}}\bar{y}_3 + \frac{R_{f2}}{R_{m3}}(\bar{y}_3 - \bar{y}_2)$$

$$+ 2\zeta_{q3}\bar{z}_3' + \frac{\zeta_3 R}{R_{m3}}\bar{z}_3 = R_{\epsilon3}R^2\cos(R\tau) \qquad (4.11)$$

$$\bar{z}_3'' + 2\zeta_3\bar{z}_3' + \frac{R_{k3}}{R_{m3}}\bar{z}_3 + \frac{R_{f2}}{R_{m3}}(\bar{z}_3 - \bar{z}_2)$$

$$- 2\zeta_{q3}\bar{y}_3' - \frac{\zeta_3 R}{R_{m1}}\bar{y}_3 = R_{\epsilon3}R^2\sin(R\tau) \qquad (4.12)$$

By choosing the state vector $\underline{x}$ to be

$$\underline{x} = [\bar{y}_1\ \bar{y}_2\ \bar{y}_3\ \bar{v}_{y1}\ \bar{v}_{y2}\ \bar{v}_{y3}\ \bar{z}_1\ \bar{z}_2\ \bar{z}_3\ \bar{v}_{z1}\ \bar{v}_{z2}\ \bar{v}_{z3}]^T \qquad (4.13)$$

the system in first-order form becomes

$$\underline{x}' = A\underline{x} + \underline{d} \qquad (4.14)$$

where

$$A = \begin{bmatrix} 0 & \vdots & I & \vdots & 0 & \vdots & 0 \\ K & \vdots & -D & \vdots & -N & \vdots & -H \\ 0 & \vdots & 0 & \vdots & 0 & \vdots & I \\ N & \vdots & H & \vdots & K & \vdots & -D \end{bmatrix} \qquad (4.15)$$

and

$$K = \begin{bmatrix} -\dfrac{(R_{k1} + R_{f1})}{R_{m1}} & \dfrac{R_{f1}}{R_{m1}} & 0 \\[3ex] \dfrac{R_{f1}}{R_{m2}} & -\dfrac{(R_{k2} + R_{f1} + R_{f2})}{R_{m2}} & \dfrac{R_{f2}}{R_{m2}} \\[3ex] 0 & \dfrac{R_{f2}}{R_{m3}} & -\dfrac{(R_{k3} + R_{f2})}{R_{m3}} \end{bmatrix} \qquad (4.16)$$

$$D = \begin{bmatrix} 2\zeta_1 & 0 & 0 \\ 0 & 2\zeta_2 & 0 \\ 0 & 0 & 2\zeta_3 \end{bmatrix} \qquad (4.17)$$

$$N = \begin{bmatrix} \dfrac{\zeta_1 R}{R_{m1}} & 0 & 0 \\ 0 & \dfrac{\zeta_2 R}{R_{m2}} & 0 \\ 0 & 0 & \dfrac{\zeta_3 R}{R_{m3}} \end{bmatrix} \qquad (4.18)$$

$$H = \begin{bmatrix} 2\zeta_{q1} & 0 & 0 \\ 0 & 2\zeta_{q2} & 0 \\ 0 & 0 & 2\zeta_{q3} \end{bmatrix} \qquad (4.19)$$

and

$\underline{d}$ = disturbance vector of unbalance and nonlinear
   bearing forces.

Characteristics of the Uncontrolled Rotor

   This section describes the characteristics of the
rotor model developed in the previous section.   Table
4.2 shows the parameter values used for this model.

   As in the previous chapter, stability can be
determined by examination of the poles of the linear
system. Fig. 4.2 shows a trace of the rotor poles for
$0 \leq R \leq 5$.   The first mode is unstable above $R = 1.78$,
the second above $R = 4.1$ and the third above $R = 4.65$.
Fig. 4.3, Fig. 4.4, and Fig. 4.5 show modal "orbit"

Table 4.1

Dimensionless Parameter Definitions

Nomenclature	Parameter	Equivalent
Frequency	ω_o	$\sqrt{\dfrac{K_t}{M_t}}$
Mass	R_{mi}	$\dfrac{m_i}{M_t}$
Damping	ζ_i	$\dfrac{C_i}{2m_i\omega_o}$
Stiffness	R_{ki}	$\dfrac{K_i + K_{si}}{K_t}$
	R_{fi}	$\dfrac{K_{fi}}{K_t}$
Cross-Coupled Damping	ζ_{qi}	$\dfrac{C_{qi}}{2m_i\omega_o}$
Cross-Coupled Stiffness	$\zeta_{si}R$	$\zeta_{si}R$
Spin Speed	R	$\dfrac{\omega}{\omega_o}$
Displacements	$\bar{y}_i, \ \bar{z}_i$	$\dfrac{y_i}{\epsilon_t}, \ \dfrac{z_i}{\epsilon_t}$
Deadband	$\bar{g}_i$	$\dfrac{g_i}{\epsilon_t}$
Time	τ	$\omega_o t$

Where: $M_t = m_1 + m_2 + m_3$, $\epsilon_t = \epsilon_1 + \epsilon_2 + \epsilon_3$, and

$K_t = K_1 + K_{s1} + K_2 + K_{s2} + K_3 + K_{s3}$

shapes for each of these modes at their respective unstable speeds. For the chosen mode, the modal orbits are obtained by combining the complex eigenvector and eigenvalue into the form of a solution and retaining the real part. These orbits show that the (mainly) rigid body "bounce" mode is the first to become unstable, followed by the rigid body "pitch" mode, and finally the flexible mode. This is the expected order, as the lower frequency (rigid) modes are most easily excited.

Table 4.2

Rotor Parameter Values

Parameter	Value
R_{m1}	0.25
R_{m2}	0.50
R_{m3}	0.25
ζ_1	0.25
ζ_2	0
ζ_3	0.25
R_{k1}	0.50
R_{k2}	0
R_{k3}	0.50
R_{f1}	0.50
R_{f2}	0.50
ζ_{q1}	0.05
ζ_{q2}	0
ζ_{q3}	0.05
$R_{\epsilon1}$	0
$R_{\epsilon2}$	1.00
$R_{\epsilon3}$	0

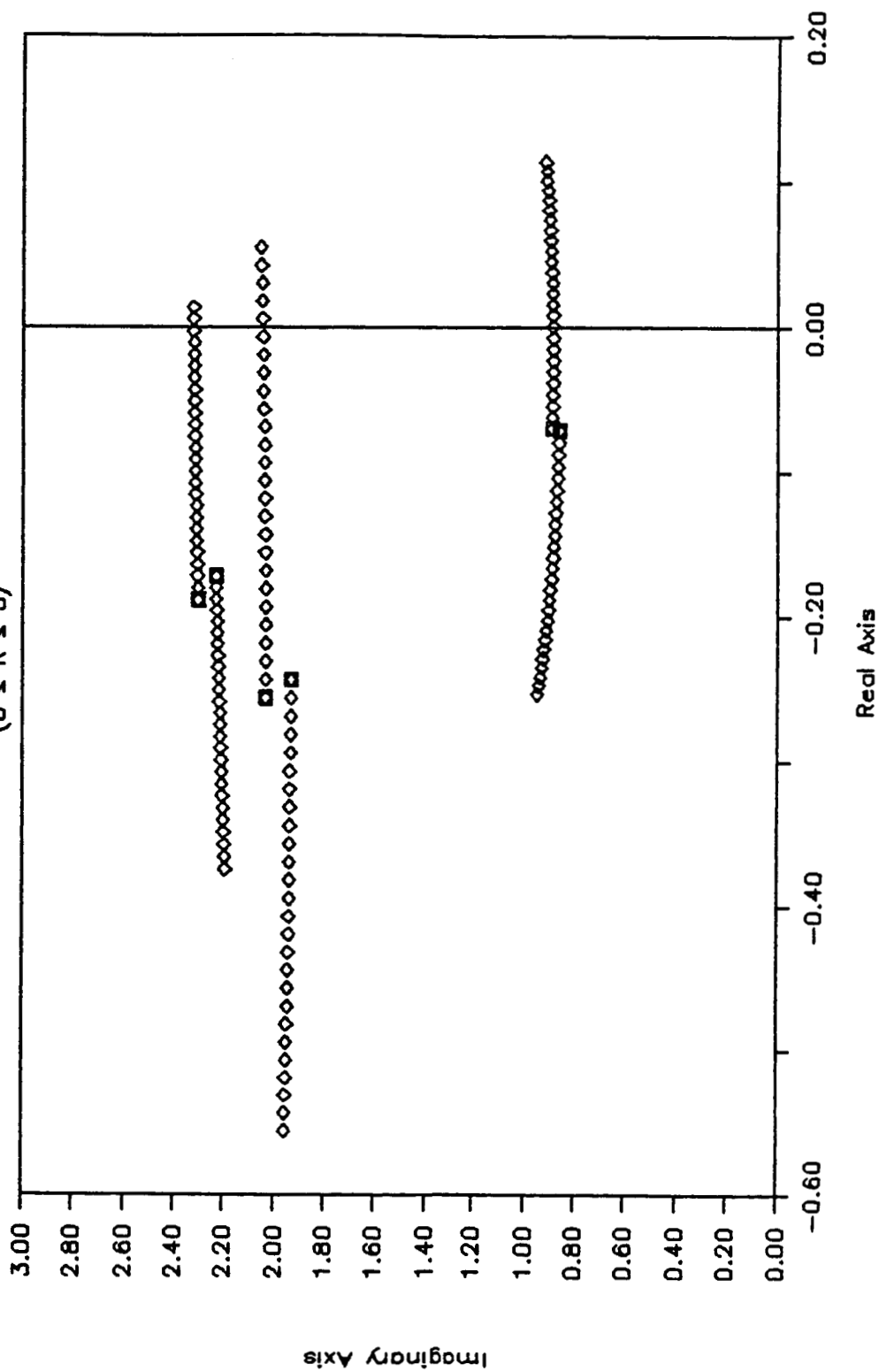Fig. 4.2. Uncontrolled Rotor Pole Trace.

MODAL ORBIT SHAPE

First Unstable Mode at R = 1.775
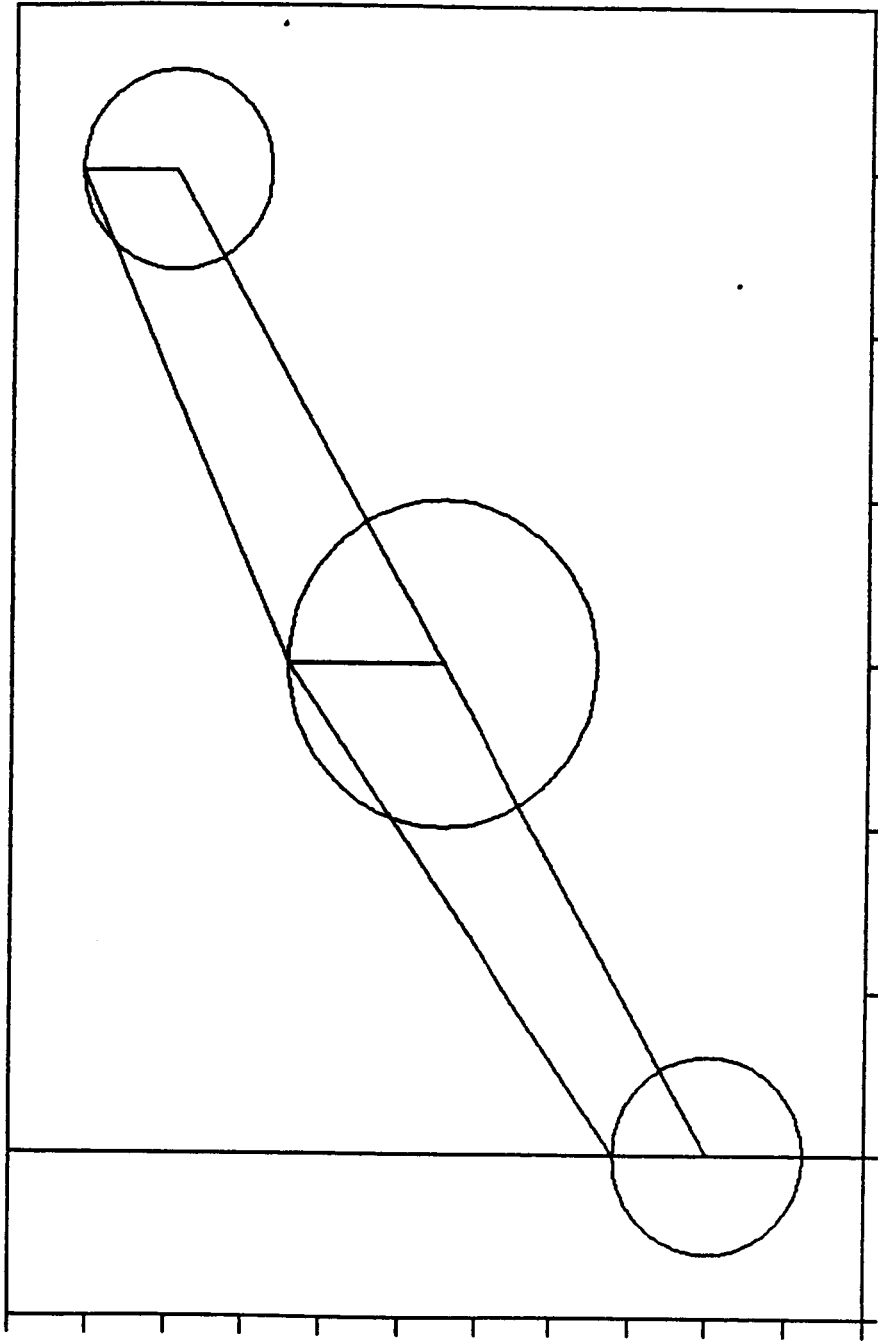
Fig. 4.3. Modal Orbit Shape of First Unstable Mode at R = 1.775.
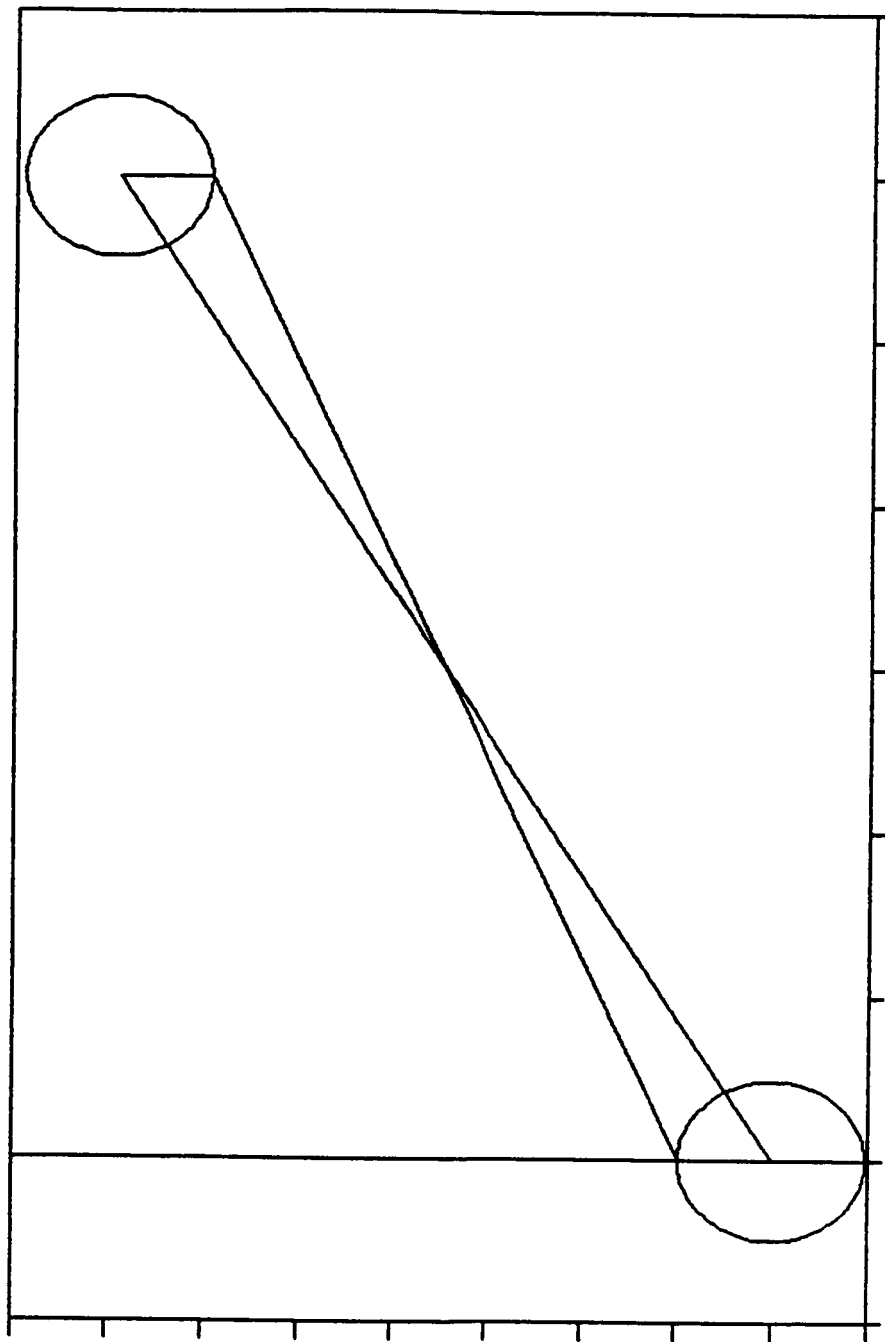
MODAL ORBIT SHAPE
Second Unstable Mode at R = 4.101

Fig. 4.4. Modal Orbit Shape of Second Unstable Mode at R = 4.101.
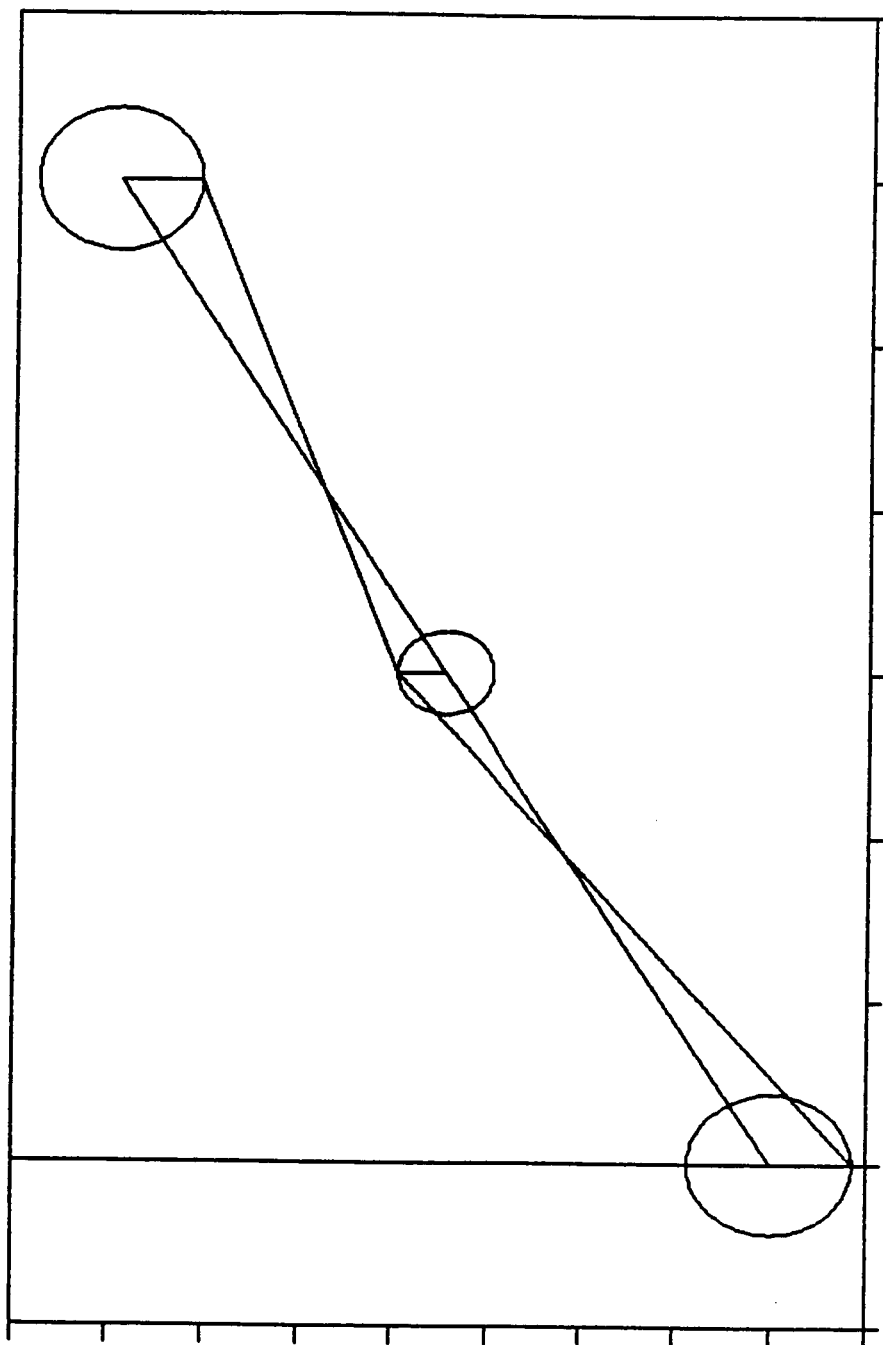
49

Fig. 4.5. Modal Orbit Shape of Third Unstable Mode at R = 4.65.

Control Structure

In this section, the control structure is developed and implemented on the linear rotor system. Disturbances are neglected. Taking the system without disturbances, the control $\underline{u}$ is added so that

$$\underline{x}' = A\underline{x} + B\underline{u}. \tag{4.20}$$

Now let

$$\underline{u} = -G\underline{y} \tag{4.21}$$

where

$$\underline{y} = C\underline{x}. \tag{4.22}$$

The above control form is chosen because full state feedback is impractical on physical rotor systems. The closed-loop system becomes

$$\underline{x}' = (A - BGC)\underline{x}. \tag{4.23}$$

To produce the two control forces

$$\underline{u} = \begin{bmatrix} u_1 \\ u_2 \end{bmatrix} \tag{4.24}$$

the gain matrix must be based on the form of the output $\underline{y}$. The output $\underline{y}$ is chosen to take the form

$$\underline{y} = [\ Y_c \ V_{yc} \ Z_c \ V_{zc} \ ]^T \tag{4.25}$$

where

Y_c is a linear combination of the Y-direction

displacements y_1, y_2, y_3,

V_{yc} is a linear combination of the Y-direction

velocities v_{y1}, v_{y2}, v_{y3},

Z_c is a linear combination of the Z-direction

displacements z_1, z_2, z_3 , and

V_{zc} is a linear combination of the Z-direction

velocities v_{z1}, v_{z2}, v_{z3}.

Obviously, there are many ways to structure the output

$\underline{y}$. The above choice is logical, however, in that it

simplifies the structure of both the output matrix C,

and the resulting gain matrix G. Recalling the radial

symmetry of the rotor, it is apparent that the Y and Z

directional measurements of the output should be symmet-

ric. This results in C having the form

$$C = \begin{bmatrix} a & b & c & 0 & 0 & 0 & 0 & 0 & 0 & 0 & 0 & 0 \\ 0 & 0 & 0 & d & e & f & 0 & 0 & 0 & 0 & 0 & 0 \\ 0 & 0 & 0 & 0 & 0 & 0 & a & b & c & 0 & 0 & 0 \\ 0 & 0 & 0 & 0 & 0 & 0 & 0 & 0 & 0 & d & e & f \end{bmatrix} . \tag{4.26}$$

Also from symmetry and the results of the previous chapter, the gain matrix G has the form

$$G = \begin{bmatrix} g_{11} & g_{12} & g_{13} & g_{14} \\ -g_{13} & -g_{14} & g_{11} & g_{12} \end{bmatrix} . \qquad (4.27)$$

The apparent difference in equation (4.27) and the gain matrix of the previous chapter results from the order of the state vector. The control distribution matrix B depends upon the chosen point of application of the control forces. It is assumed that both forces will be applied at one mass only.

Control Determination

To stabilize the rotor represented by the closed-loop system of equation (4.23), it is sufficient to position all of the poles in the left half plane. It is not necessary, however, to place all the poles to achieve stability. Thus, the system of equation (4.23) need not be completely controllable. By using one magnetic bearing set in the absence of full state feedback, the control is suboptimal.

The various analytical techniques available for dealing with the linear suboptimal control problem generally influence a portion of the system in a specific way, and minimize the influence of the control on the

remainder of the system. Modal control, for example, "fine-tunes" a specific mode or modes, while the "spill-over" of the control to other modes is not directly controlled. The use of this technique for this application limits the number of directly controllable modes to one. While this allows the rotor to operate above previously unstable speeds, the influence of the control on the two remaining modes would be questionable.

For these reasons, a direct search method for determining the control gains is used. Using Powell's method [15] a function is minimized by iteratively searching an independent vector, in this case, the control gains. As discussed in the previous chapter, a useful measure of the stability of the system is the relative damping of the systems's modes. The relative damping ζ_{RD} of the ith mode is defined as before to be

$$\zeta_{RD}i = \frac{-\delta_i}{\sqrt{\delta_i^2 + \omega_i^2}} \qquad (4.28)$$

where $\lambda_i = \delta_i \pm j\omega_i$ is the eigenvalue associated with that mode. It is the minimum relative damping which is critical to the stability of the system. Maximizing that minimum relative damping is equivalent to maximizing the shaded region of Fig. 4.6. The minimum relative damping of the closed-loop system is determined by a computational function. The negative of this function

is minimized using Powell's method to determine the control gains. The applications of this approach are discussed in the next section.
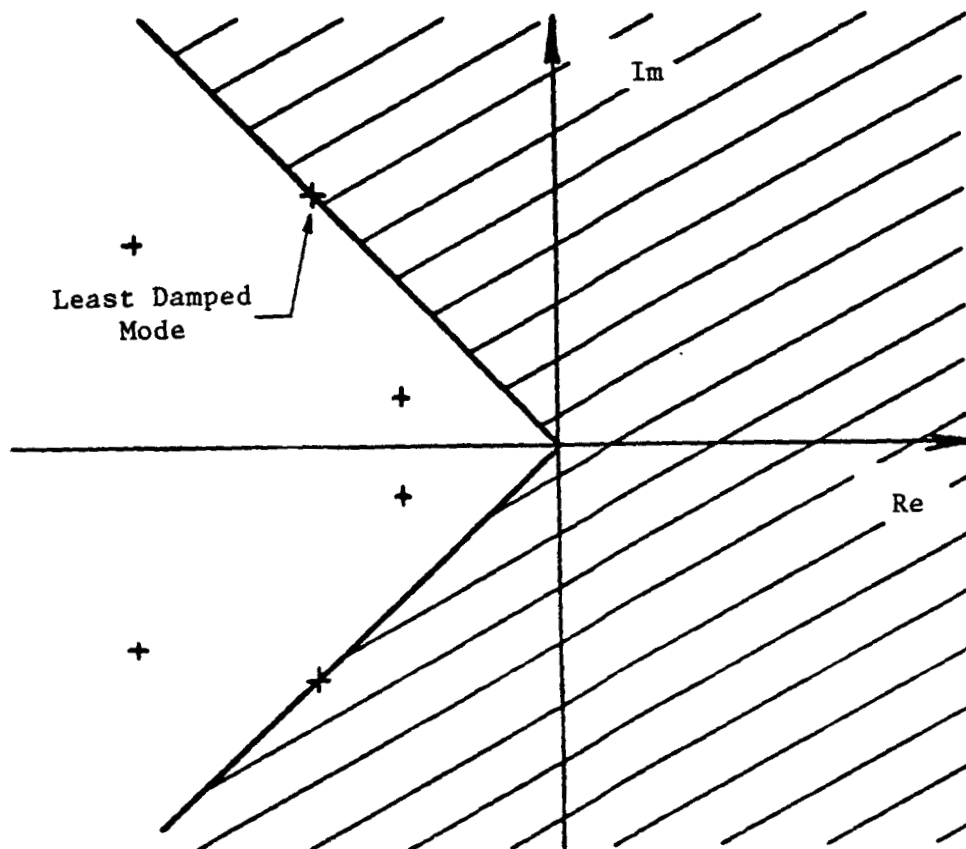

Fig. 4.6. Effect of Maximizing ζ_{RD}

Control Application

Before the control gains are determined, two factors must be specified concerning the control:

   (1) Point of application of the bearing,

   (2) Combination of measurements for the output signal.

To best determine the location for applying the control, it is useful to examine the uncontrolled rotor's modal orbit shapes. Recalling Fig. 4.3 through Fig. 4.5, it can be seen that, for affecting the first unstable mode (Fig. 4.3), the bearing can be located at either three mass positions. This is because that mode is very nearly a rigid body translational (or "bounce") mode. Examination of the next unstable mode (Fig. 4.4) clearly shows that a bearing located at the center mass location offers no stabilizing effect for this mode. Since this mode is unstable at a speed lower than the third mode, controlling it takes priority over modes that follow. Therefore, the magnetic bearing should be located at an end mass location, say that of m_1.

The decision of where to measure and how to combine the signals for the output y is not as simple as the location of the control. It is helpful to make a restriction regarding this factor. Since full state feedback is impractical for most rotor systems, it is assumed that the information from all three mass

locations will not be available. The output can contain information from two locations, at most. An examination of the uncontrolled rotor's modal orbit shapes shows that if information is provided from the center mass location only, the second ("pitch") mode cannot be affected. Thus, an end location must be measured. For stabilization of the third mode, information from the center mass is required as well. To gain more insight into the question of measurement, the search program was run for varying combinations of measuring locations. For each trial, the stabilization capabilities were observed. The results of these show that the best degree of stabilization is obtained from signal measurement at the center mass location and the end location where the magnetic bearing is to be located. Furthermore, by appropriate weighting of the measurements an even higher degree of stabiliztion is achieved.

Using the end mass m_1 as a location for the magnetic bearing and measuring the displacement and velocity signals at the end and center masses m_1 and m_2 with

$$
C = \begin{bmatrix}
2 & 1 & 0 & 0 & 0 & 0 & 0 & 0 & 0 & 0 & 0 & 0 \\
0 & 0 & 0 & 2 & 1 & 0 & 0 & 0 & 0 & 0 & 0 & 0 \\
0 & 0 & 0 & 0 & 0 & 0 & 2 & 1 & 0 & 0 & 0 & 0 \\
0 & 0 & 0 & 0 & 0 & 0 & 0 & 0 & 0 & 2 & 1 & 0
\end{bmatrix} ,
$$

the search program was used to determine the control
gains. For various spin speeds the gains were computed
to maximize the relative damping. For the chosen output
and bearing location, the rotor was stabilized for
speeds up to approximately $R = 7.2$. Fig. 4.7 shows the
control gains obtained over the speed range $0 \leq R \leq 8$.
This figure illustrates that for any given speed, there
are numerous solutions which optimize the damping.
Using the gains obtained from a prior speed as starting
values and incrementing the speed slightly, it was pos-
sible to "track" a particular solution over the speed
range. The irregularities observable in the figure,
however, show the difficulties associated with this
approach.

The poles of the controlled rotor system using the
gains of Fig. 4.7 are shown in Fig. 4.8. Enlarged views
of various sections are shown in Fig. 4.9 through
Fig. 4.11. Due to the somewhat irregular nature of the
control gain solutions, the behavior of the poles, espe-
cially at lower speeds, is somewhat erratic.

For comparison, the control gains from Fig. 4.7 at
the stability threshold speed ($R = 7.2$) are used and
held constant over the entire speed range. Fig. 4.12
shows the rotor poles for these constant gains. As seen
in the enlarged views of Fig. 4.13 through 4.15, the

poles are more well behaved than those obtained using speed dependent gains. More importantly, however, is the fact that the system is stable over the same speed range. A close comparison of Fig. 4.8 with Fig. 4.12 reveals that the overall behavior of the poles does not differ significantly. This indicates that, at least for this model, there is little advantage to using speed dependent gains. Therefore, the rest of this chapter will deal with systems controlled by the constant gains obtained at $R = 7.2$

Fig. 4.7. Control Gains Vs. Spin Speed.

CONTROLLED ROTOR POLES

(0 ≤ R ≤ 8)
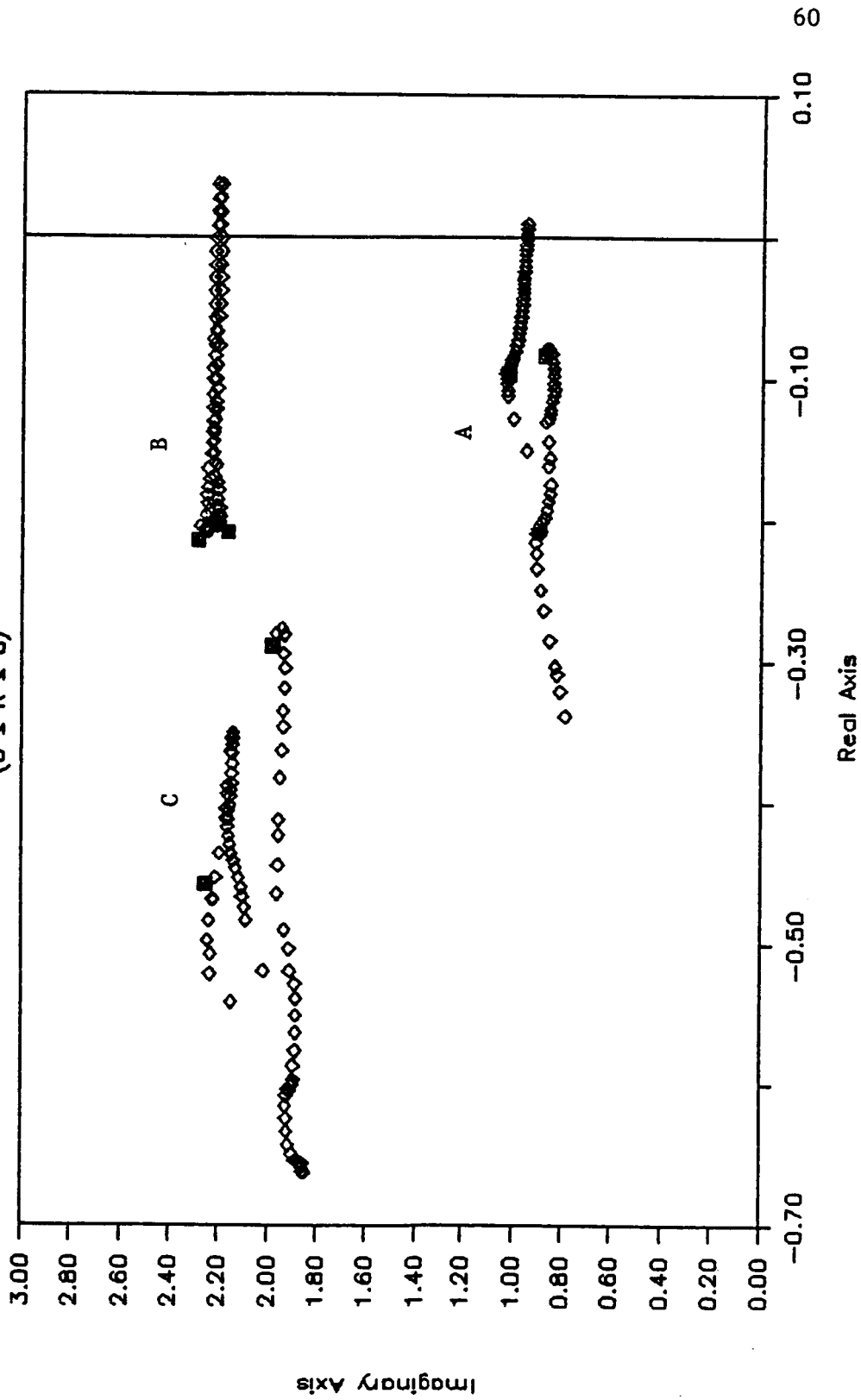
Fig. 4.8. Controlled Rotor Pole Trace with Speed Dependent Control.

Fig. 4.9. Controlled Rotor Pole Trace with Speed Dependent Gains, Section A Enlarged.

62
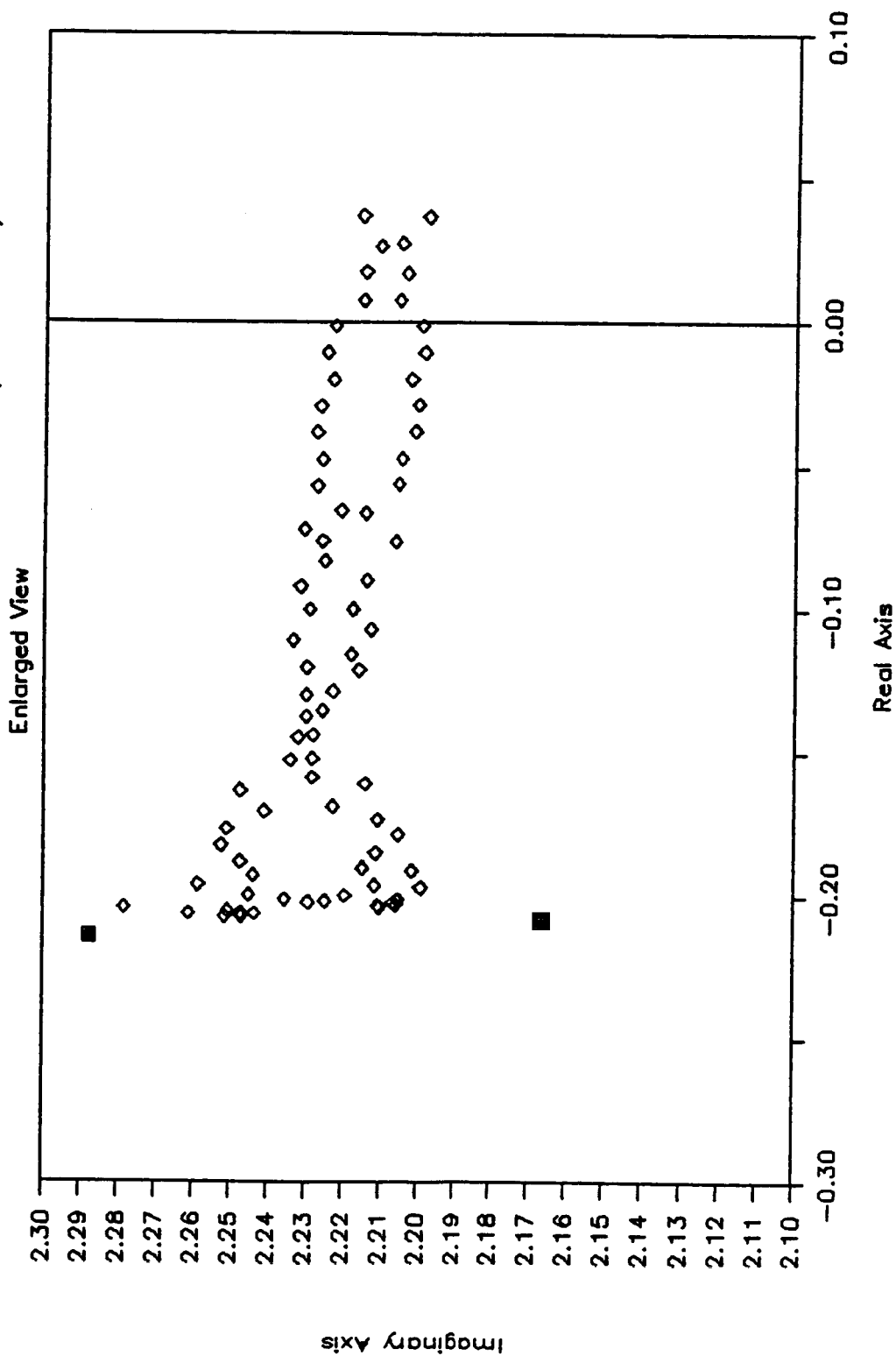
Fig. 4.10. Controlled Rotor Pole Trace with Speed Dependent Gains, Section B Enlarged.
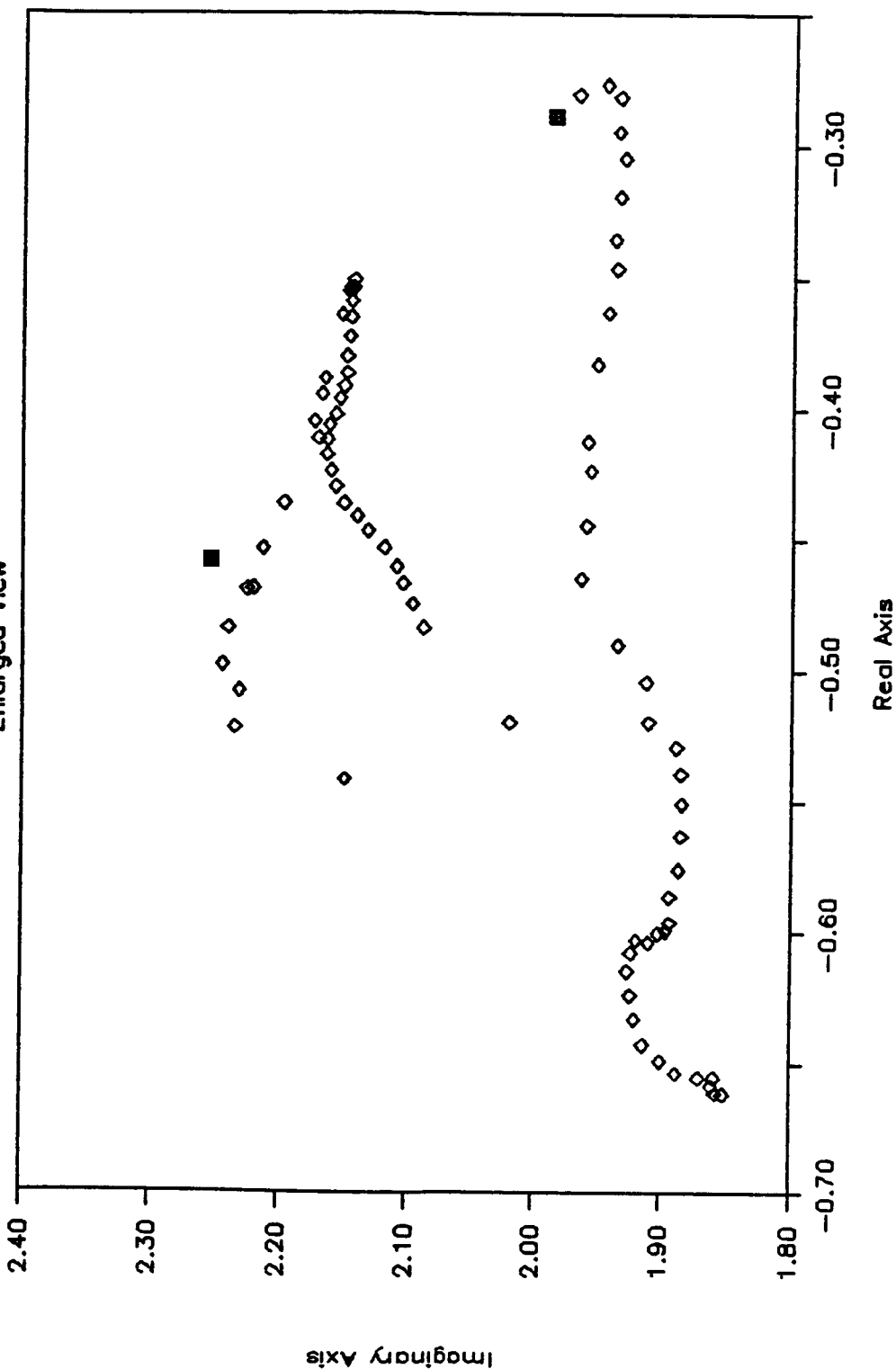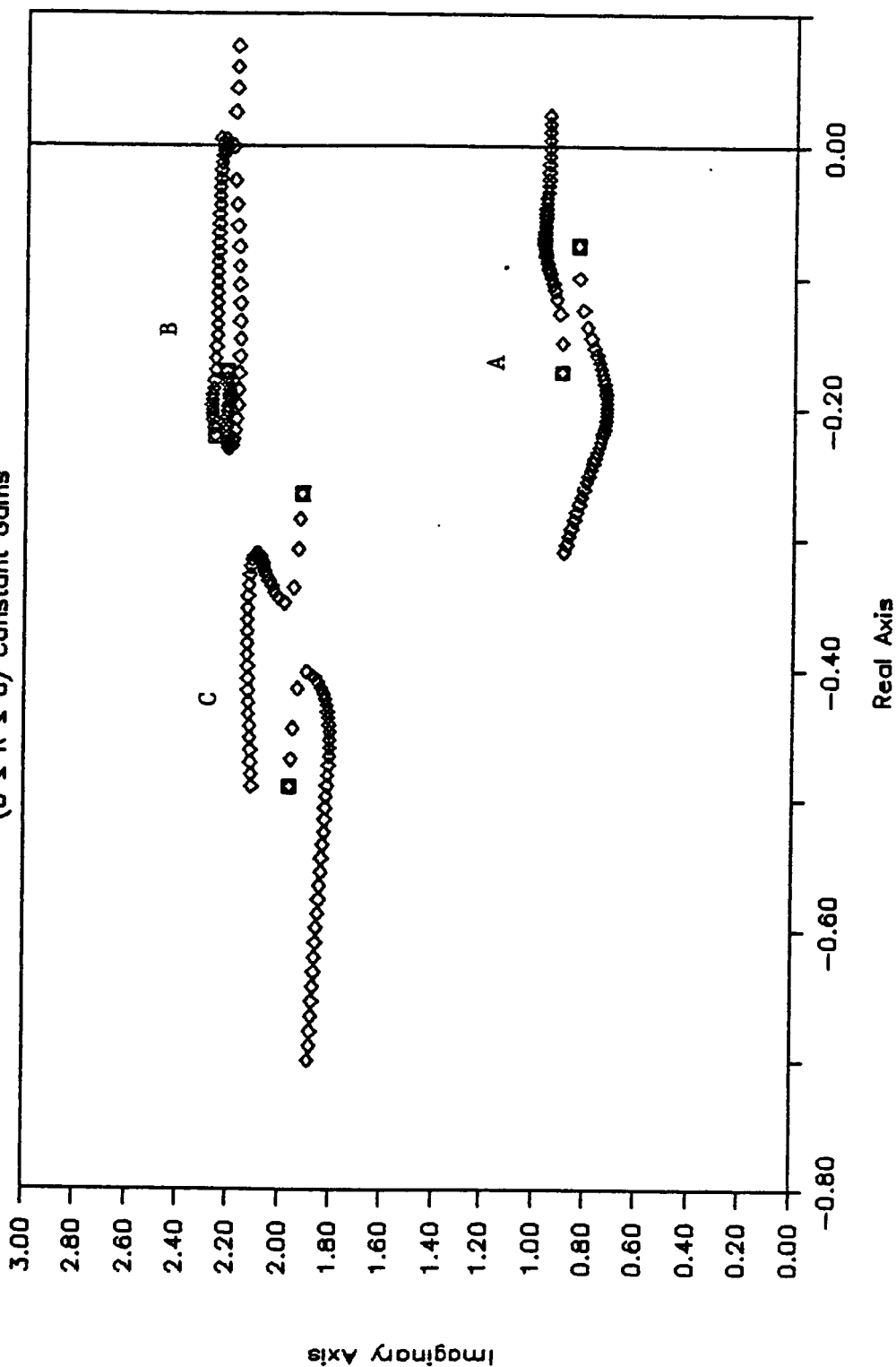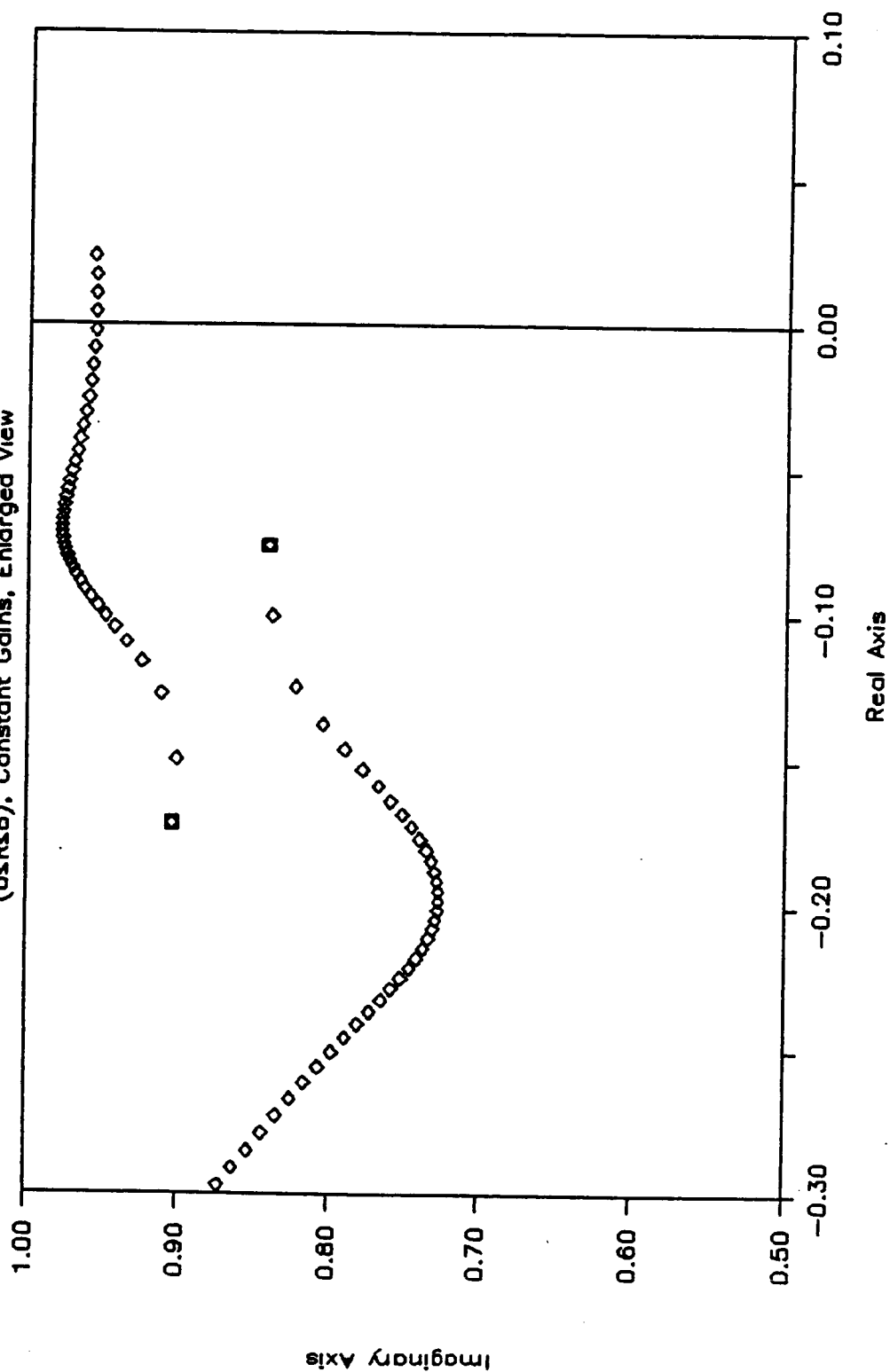
CONTROLLED ROTOR POLES ($0 \leq R \leq 8$)

Enlarged View

Imaginary Axis

Real Axis

Fig. 4.11. Controlled Rotor Pole Trace with Speed Dependent Gains, Section C Enlarged.

CONTROLLED ROTOR POLES

(0 ≤ R ≤ 8) Constant Gains

Imaginary Axis

Real Axis

Fig. 4.12. Controlled Rotor Pole Trace with Constant Gains.

Fig. 4.13. Controlled Rotor Pole Trace with Constant Gains, Section A Enlarged.

Fig. 4.14. Controlled Rotor Pole Trace with Constant Gains, Section B Enlarged.

CONTROLLED ROTOR POLES

(0≤R≤8), Constant Gains, Enlarged View

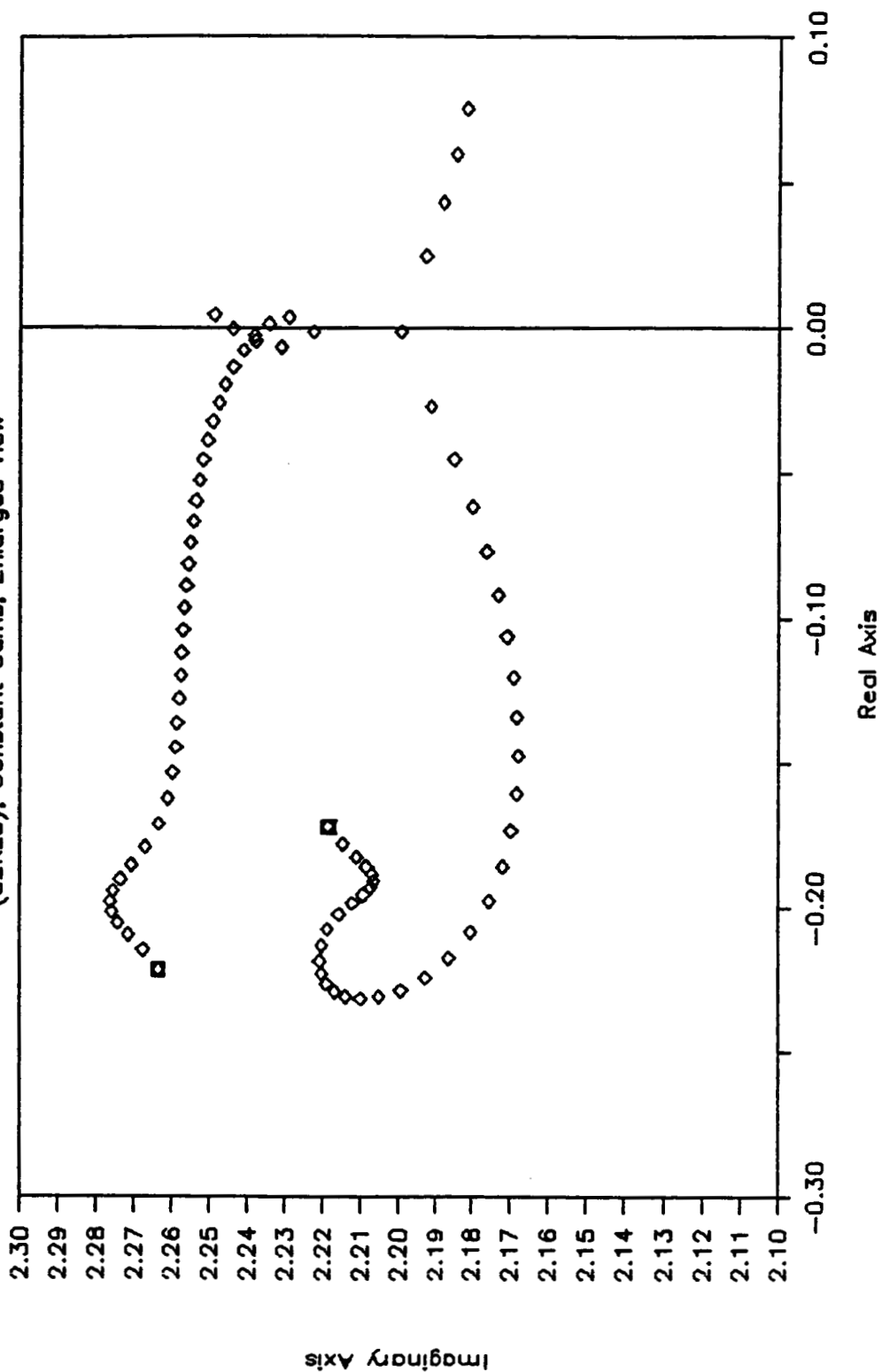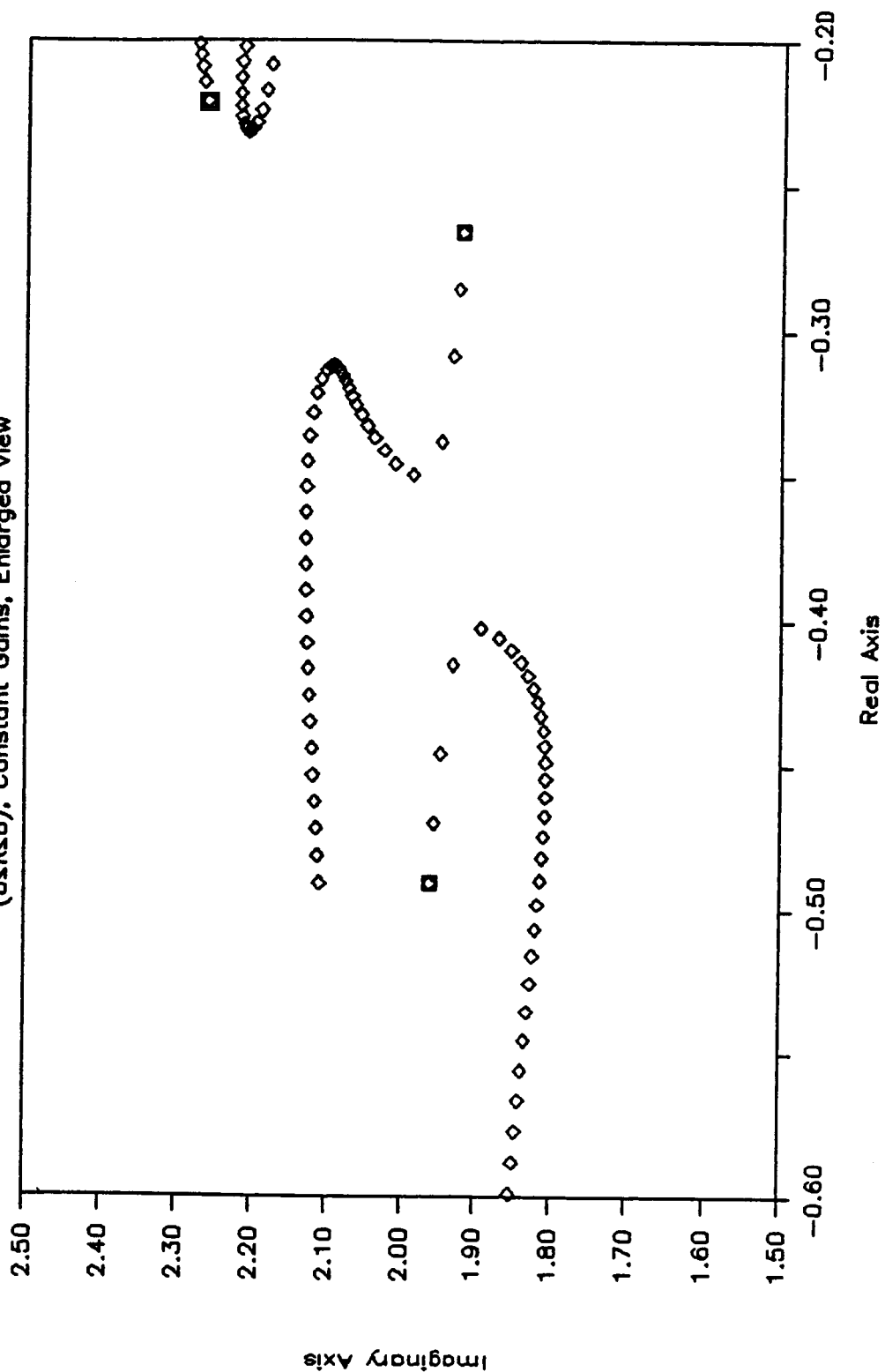Fig. 4.15. Controlled Rotor Pole Trace with Constant Gains, Section C Enlarged.

Control Performance

The performance of the control is evaluated by examining the maximum control force required to achieve stabilization. This control force is obtained by simulating the rotor at steady state, or in a limit cycle if one exists. Both the linear and nonlinear rotors are simulated. A power spectral density of a nonlinear simulation reveals its frequency components.

Fig. 4.16 shows the maximum control force required to stabilize the rotor over the speed range $0 \le R \le 6$. Though the rotor is stable for speeds up to $R = 7.2$, the amplitudes of vibration become unrealistically large as this speed is approached. For the nonlinear systems, the deadband g is equal in both the end supporting bearings. Fig. 4.16 shows that, as deadband increases, the force required to stabilize the rotor does also. The slight peak in the force curves for $\bar{g} = 0$ and $\bar{g} = 1$ occurs at a speed slightly less than $R = 1$. This is approximately the same as the first critical speed. Comparison of Fig. 4.16 with the corresponding plot of the previous chapter (Fig. 3.7) shows that nearly the same level of force is required for this model with the exception of that for the $\bar{g} = 10$ case, which for this model requires an order of magnitude greater force.

A typical simulation of the nonlinear system with $\bar{g} = 1$ is shown in Fig. 4.17 through Fig. 4.19. At $R = 2$

this system exhibits mainly synchronous motion. Increasing the speed to R = 6, as shown in Fig. 4.20 through Fig. 4.22 changes the system dramatically. While the center mass exhibits mainly synchronous motion, the end masses exhibit complex subsynchronous motions. This results from the self-exciting mechanisms being located at both end masses, and none at the center. In all cases, the amplitudes at the mass where the control is applied are significantly lower than at the other masses. Fig. 4.23 shows the frequency components of the end mass response indicating mainly subsynchronous motion. The response of the rotor with g = 10 at R = 6.0 can be seen on Fig. 4.24 through Fig. 4.26. High amplitude subsynchronous motion is clearly evident, resulting in high required control forces to maintain stability.

Summary

In this chapter, a six degree-of-freedom model was presented and stabilized to the maximum possible speed. The control was supplied by one magnetic bearing set, optimally located by examining the rotor's modal orbit shapes. For the model parameters chosen, this location was found to be the end mass of the rotor. The output measurement combination for the highest degree of stabilization combined the signals from the center mass and

the end mass where the magnetic bearing was located. The control gains were determined by use of a search method which maximized the damping of the least damped mode. Speed dependent gains offered little improvement over constant gains for this model. All three natural modes could be stabilized for speeds up to R = 7.2, which resulted in nearly a 300% increase in the threshold speed of the original rotor. The control forces required to achieve stabilization were determined for various spin speeds and bearing deadband values, and were found to increase with increasing speed and bearing deadband. Though the magnitudes of these forces grew relatively large as the threshold speed was approached, their magnitudes for the linear and low value ($\bar{g}$ = 1) deadband systems were comparable to those found for the two degree-of-freedom model for speeds up to three times that of the original threshold speed.
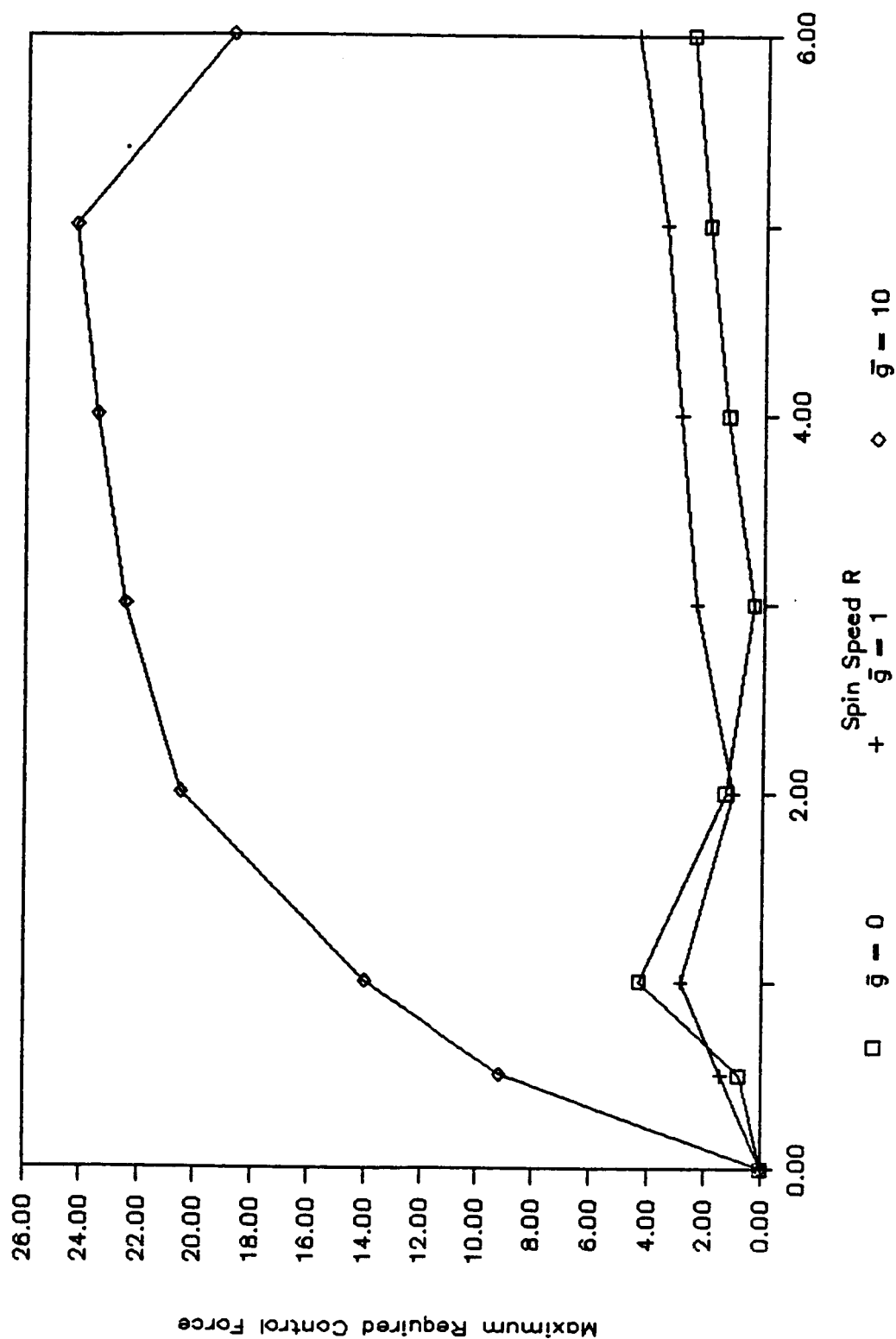
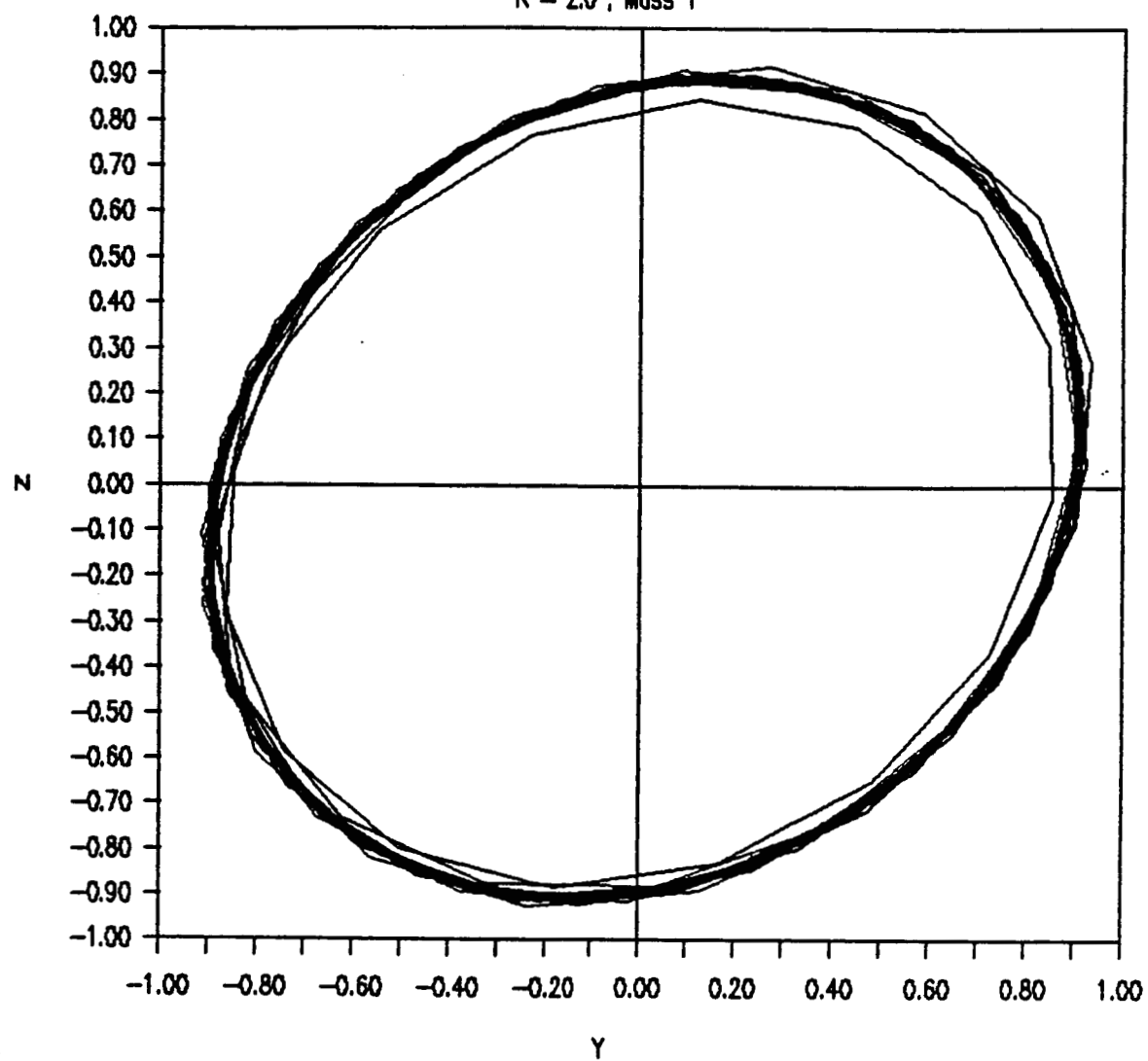Fig. 4.16. Maximum Required Control Force Vs. Spin Speed.

ROTOR CENTER POSITION

R = 2.0 , Mass 1

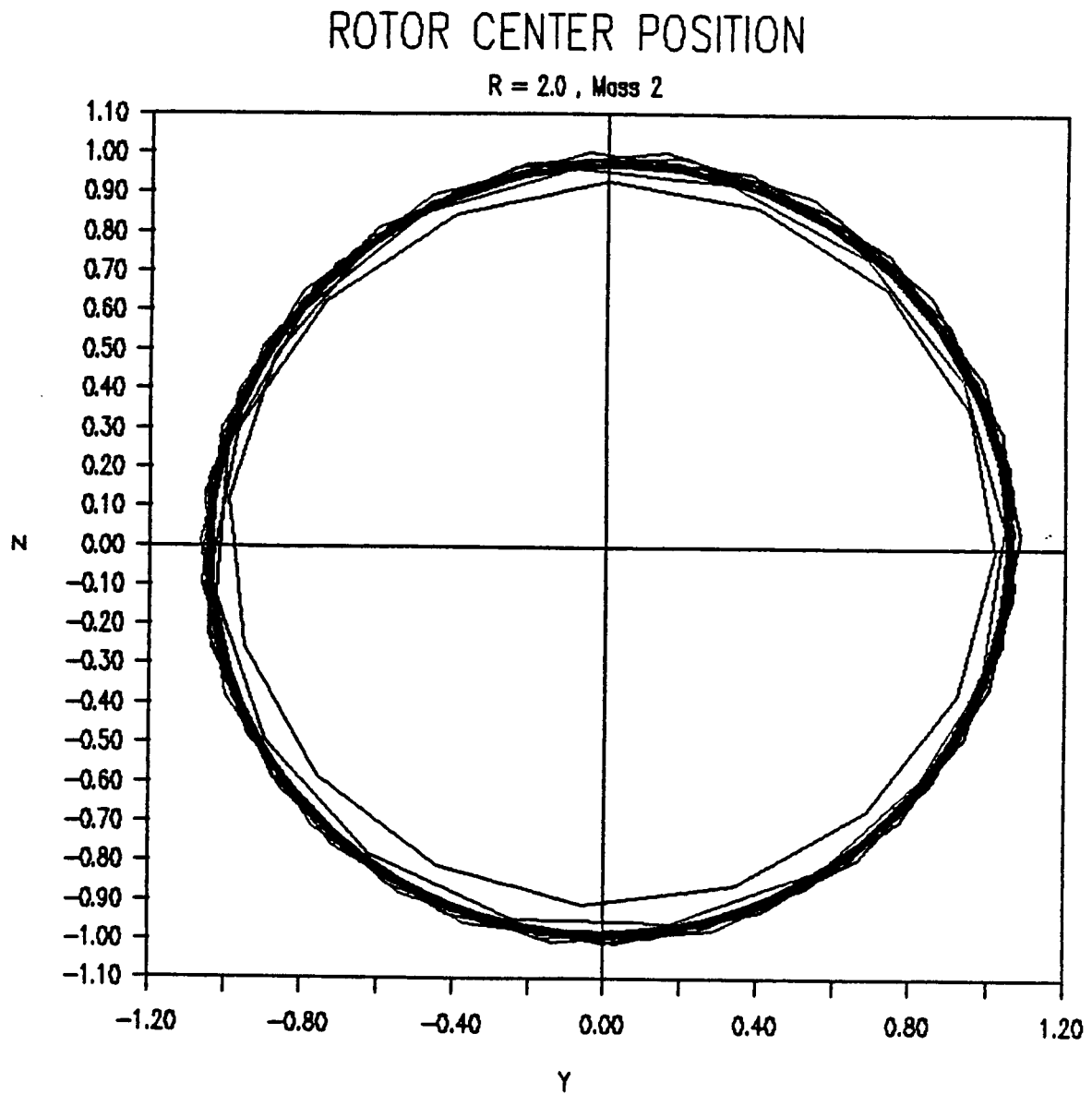Fig. 4.17. Rotor Response at Mass 1 for R = 2, $\bar{g}$ = 1.

ROTOR CENTER POSITION

R = 2.0 , Mass 2

Fig. 4.18. Rotor Response at Mass 2 with R = 2, $\bar{g}$ = 1.

ROTOR CENTER POSITION

R = 2.0 , Mass 3
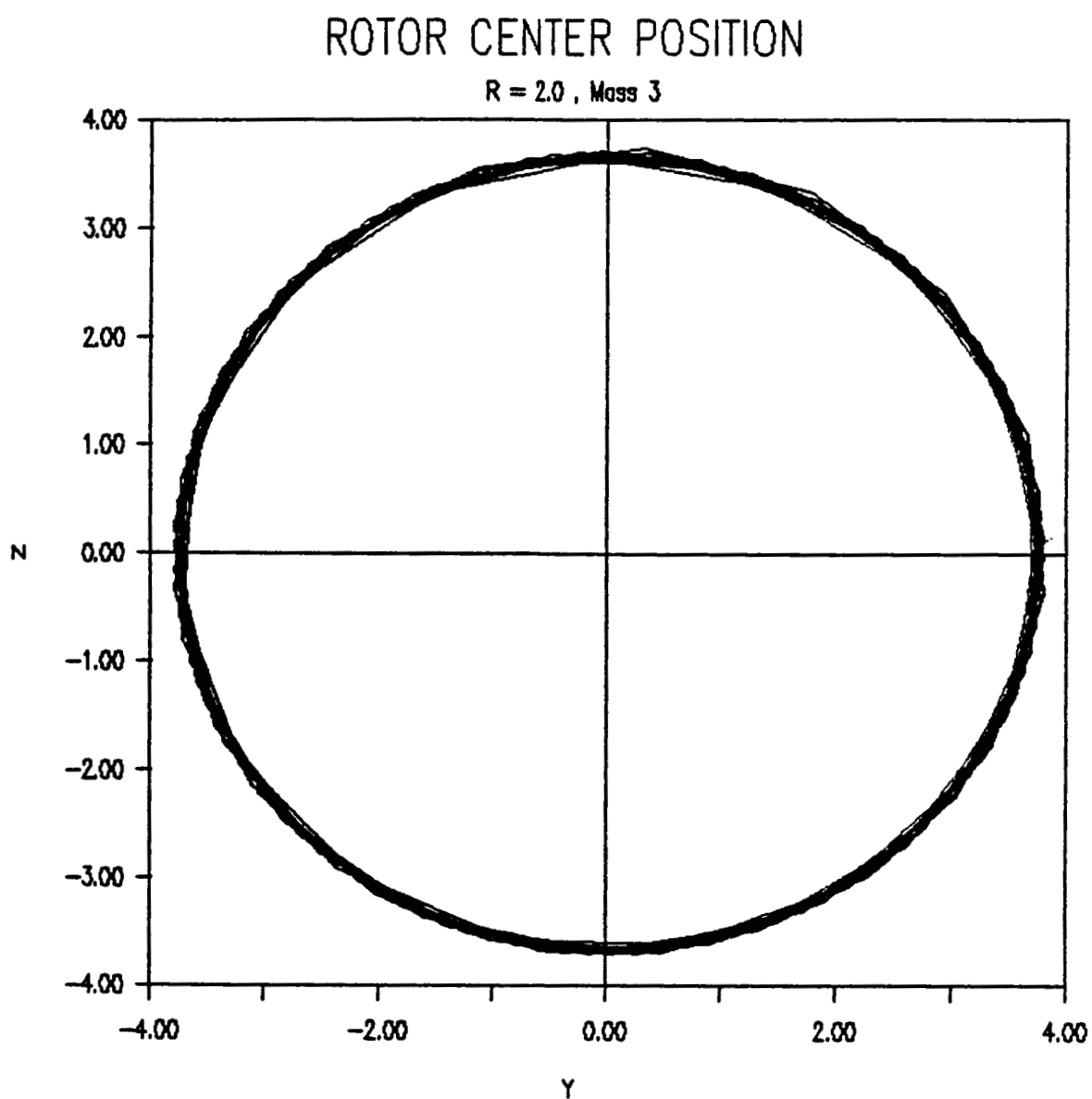
Fig. 4.19.   Rotor Response at Mass 3 with R = 2, $\bar{g}$ = 1.

ROTOR CENTER POSITION

R = 6.0 , Mass 1
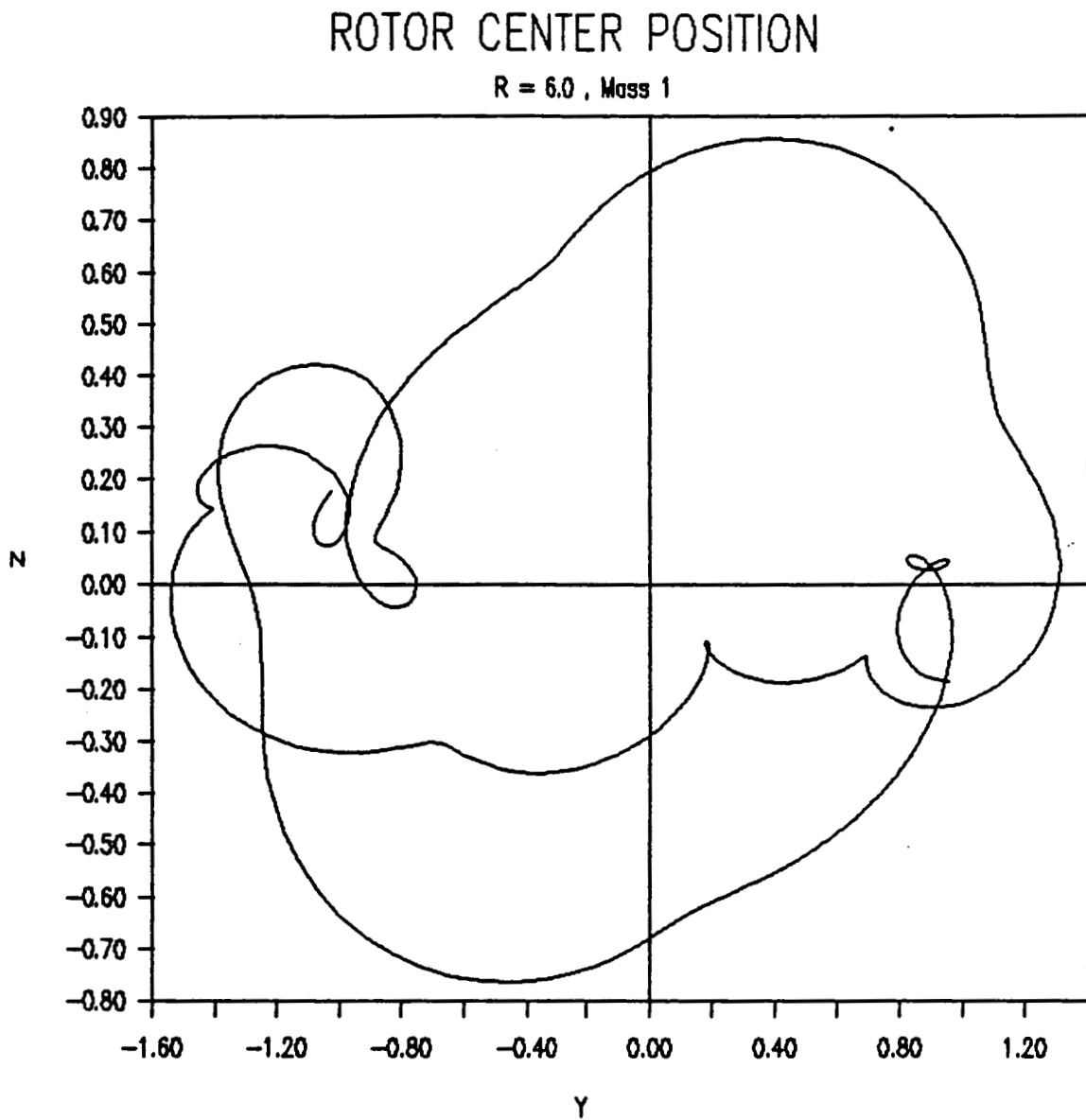
Fig. 4.20. Rotor Response at Mass 1 with R = 6, $\bar{g}$ = 1.

ROTOR CENTER POSITION

R = 6.0 , Mass 2
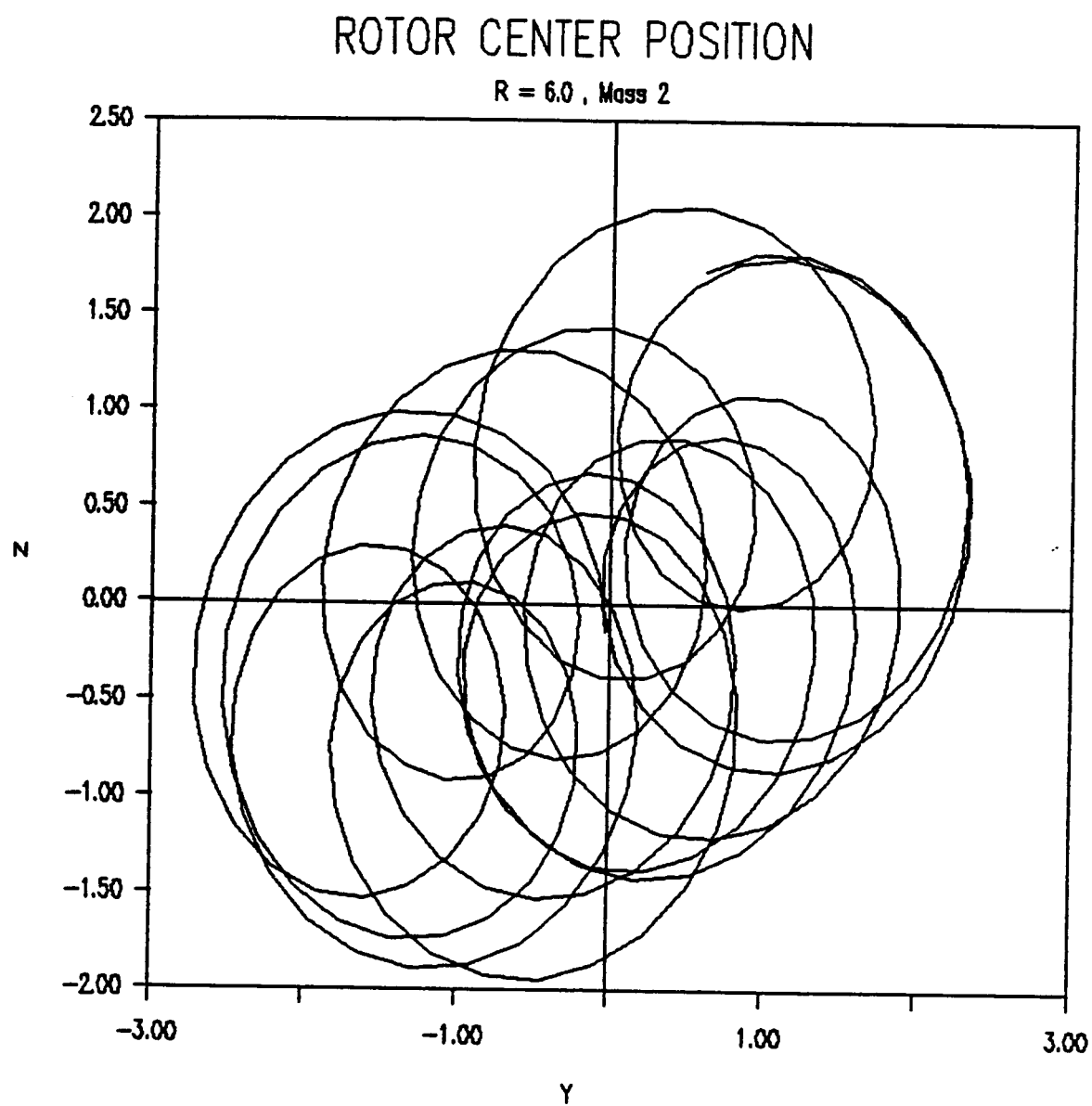
Fig. 4.21. Rotor Response at Mass 2 with R = 6, $\bar{g}$ = 1.

ROTOR CENTER POSITION

R = 6.0 , Mass 3
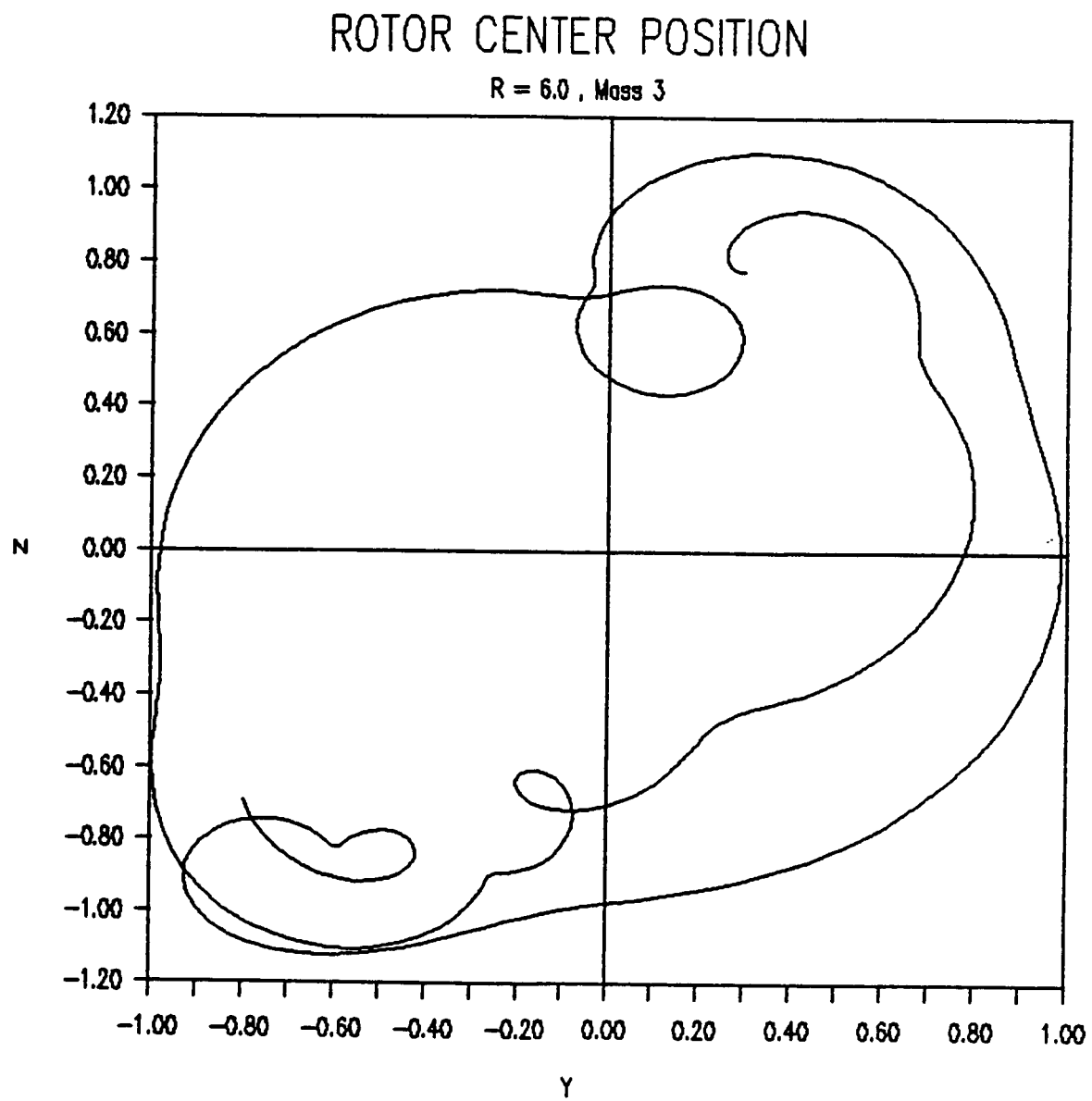

Fig. 4.22. Rotor Response at Mass 3 with R = 6, $\bar{g}$ = 1.

POWER SPECTRAL DENSITY

Response at Mass 1, R = 6.0, ḡ = 1
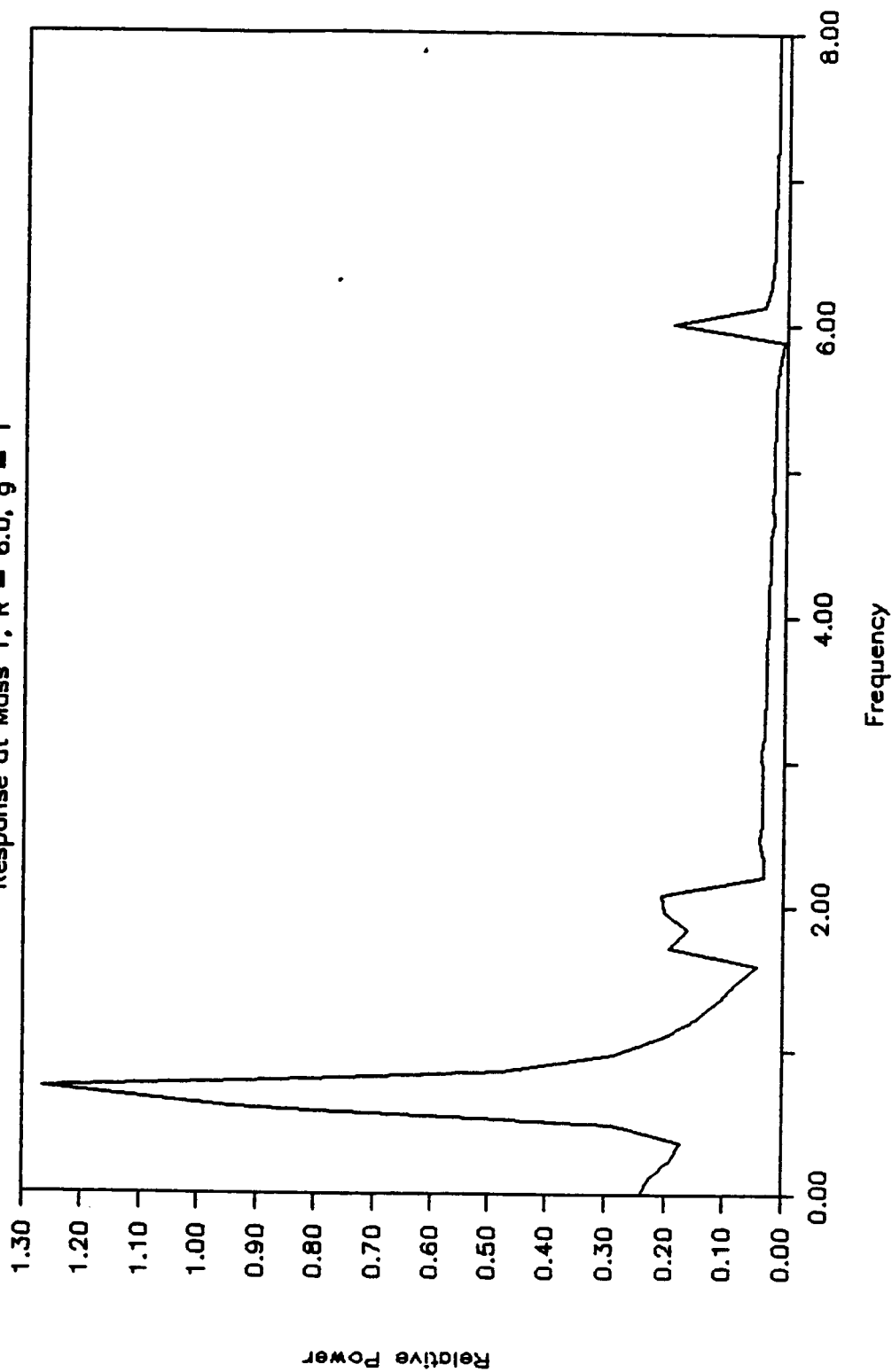
Fig. 4.23. Power Spectral Density of Response of Fig. 4.20.

ROTOR CENTER POSITION

R = 6.0 , Mass 1
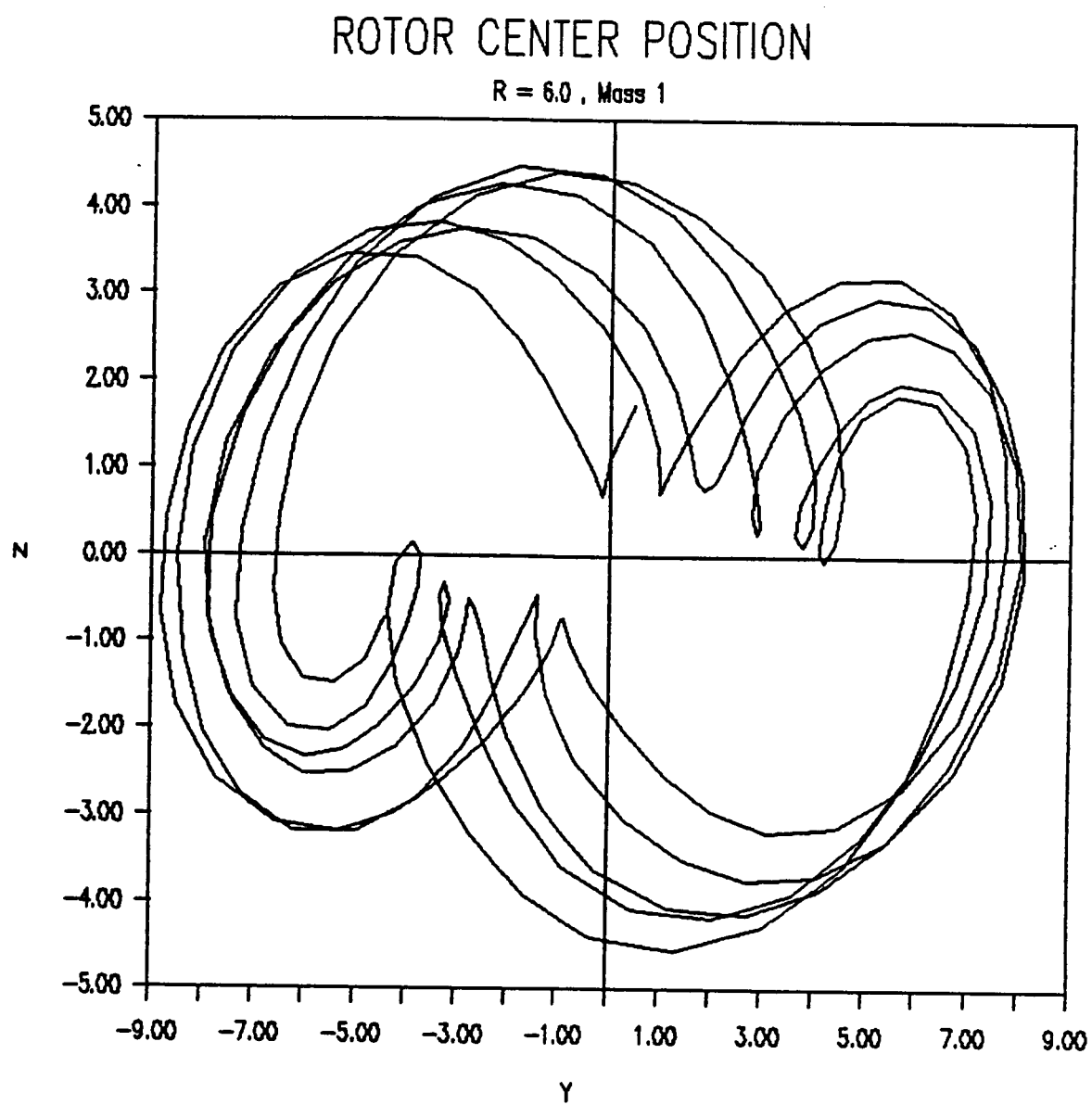
Fig. 4.24. Rotor Response at Mass 1 with R = 6, $\bar{g}$ = 10.

ROTOR CENTER POSITION

R = 6.0 , Mass 2
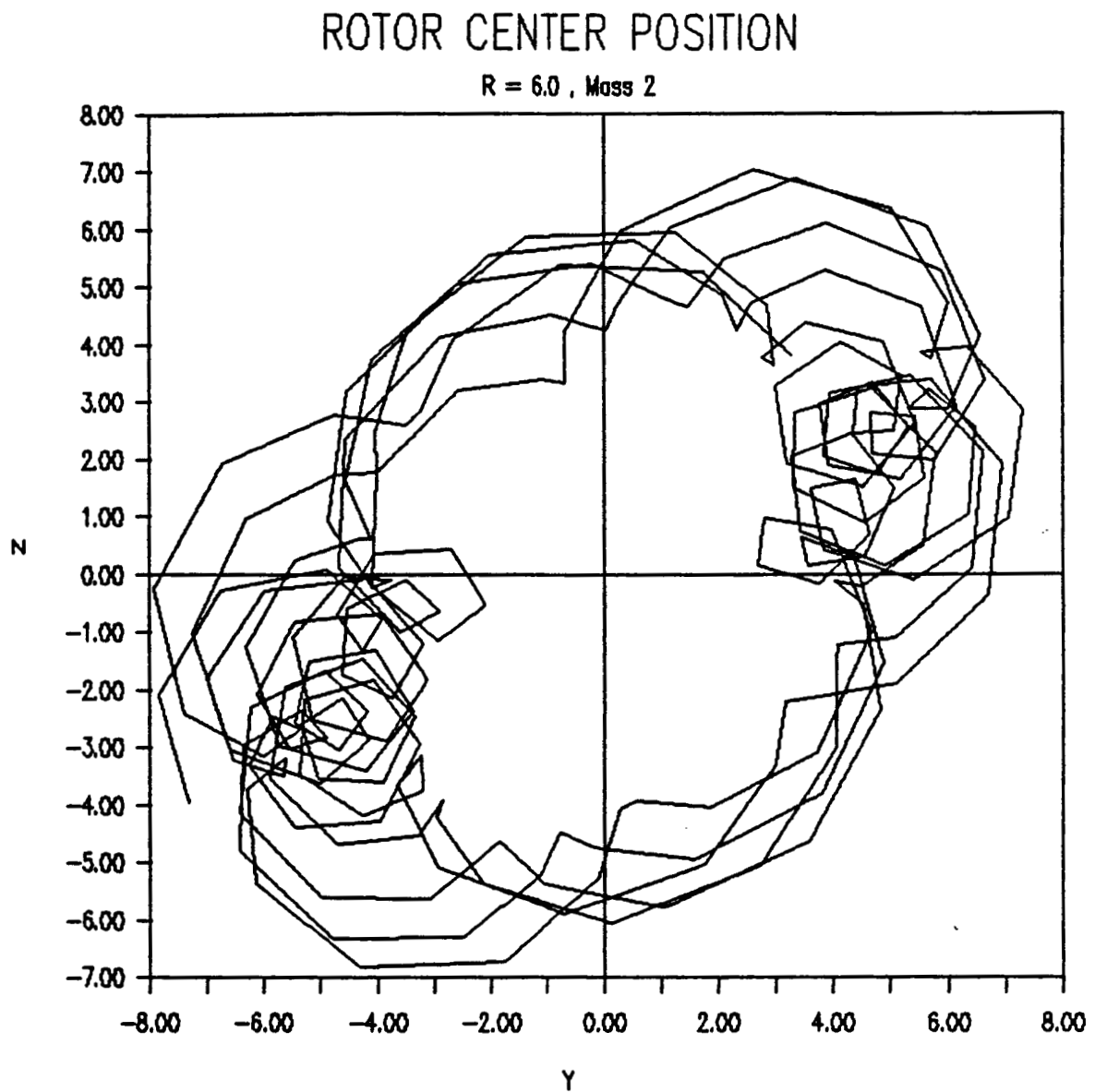
Fig. 4.25. Rotor Response at Mass 2 with R = 6, $\bar{g}$ = 10.

ROTOR CENTER POSITION
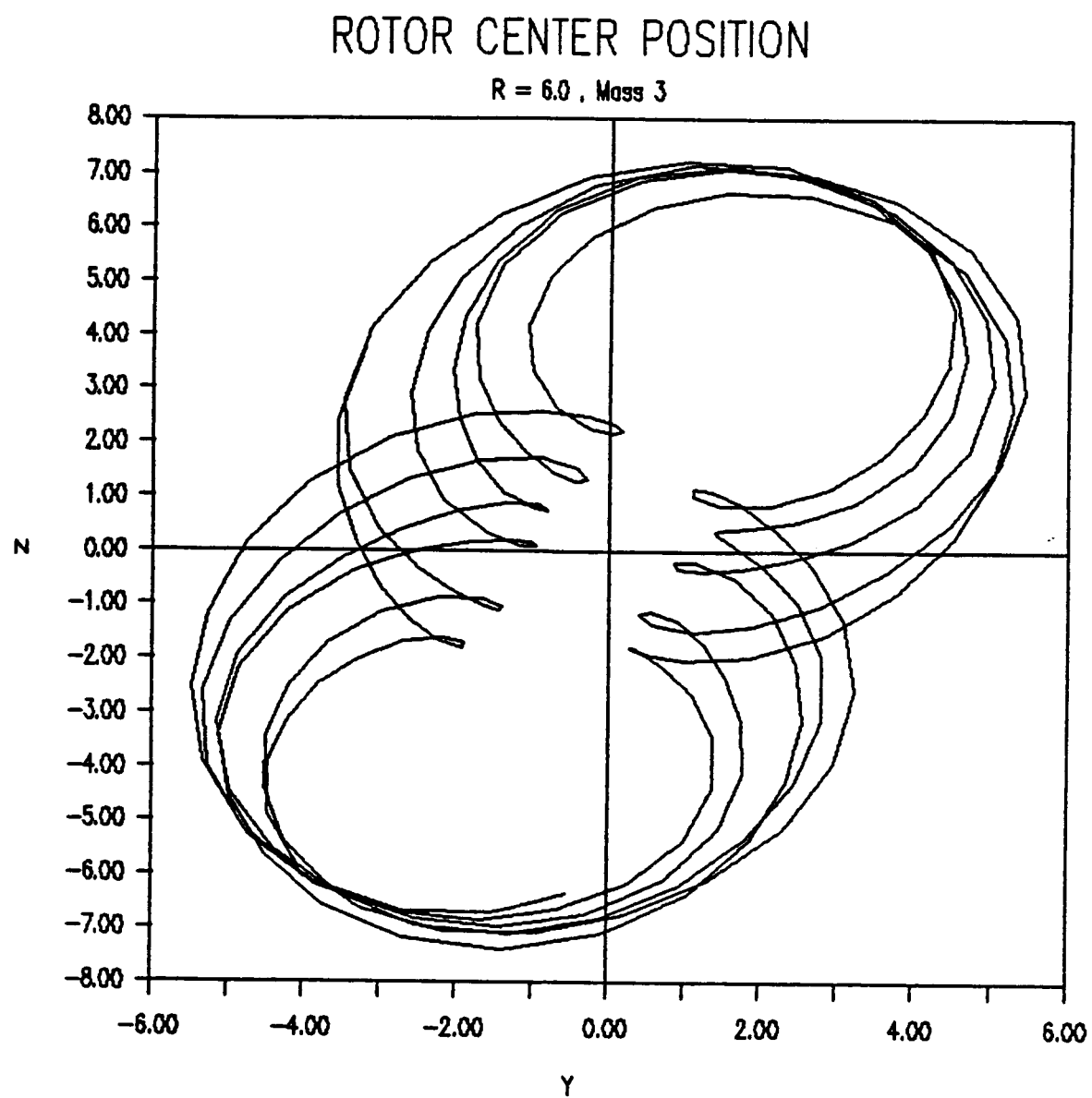
R = 6.0 , Mass 3

Fig. 4.26. Rotor Response at Mass 3 with R = 6, $\bar{g}$ = 10.

CHAPTER V

CONCLUSIONS

Using active control, the stabilization of
self-excited rotor systems has been investigated. Two
different rotor models have been used, and linear
and nonlinear cases of each examined. For each case,
the applied control has enhanced the stability charac-
teristics of the rotor significantly, allowing it to
operate above otherwise unstable speeds.

For the two degree-of-freedom model, the control
was structured to counteract self-exciting forces. In
the absence of these destabilizing forces, the rotor was
stabilized for any spin speed. The control forces
required to maintain stability were found to vary nearly
linearly with spin speed, and were not significantly
affected by bearing deadband. While this control
approach seemed somewhat simplistic, it was shown to be
quite effective. The versatile nature of magnetic bear-
ings could allow implementation of such a control scheme
in a physical rotor, especially where dimensions would
permit locating a magnetic bearing near each major self-
exciting mechanism.

82

The control approach used for the six degree-of-freedom model was shown to be effective at improving the stability of the rotor, although the improvement was limited. The system was stabilized for speeds up to nearly 300% of the original instability threshold speed. The significant result was the stabilization of each of the rotor's three natural modes using one magnetic bearing. The placement of the magnetic bearing was such that it maximized the effect that the bearing could exert on each of the rotor's natural modes. The feedback signal for the control was structured to be a composite output signal, with less than full state information. To offer the most system improvement, it was found that this signal should contain information from at least the center mass location and end mass location where the bearing was located. The control forces required to stabilize the rotor were shown to increase nonlinearly with spin speed and deadband. However, the relative magnitudes of these forces were comparable to those found for the two degree-of-freedom model. Obviously, the particular parameters chosen to describe the model affect the improvement capabilities of the control. However, in many cases even a small improvement in the stability threshold speed is worthwhile goal.

Several interesting topics relating to this study remain to be addressed. First, the function used to

determine the optimal control gains for the six degree-of-freedom model in this study was somewhat poorly suited for iterative methods. The parameter being maximized, the minimum relative damping, was a value associated with only one eigenvalue. As the eigenvalues "moved" under the effect of the control, the one with which the relative damping was associated would switch. This led to there being many solutions for the optimal gains, and erratic behavior of the eigenvalues under speed dependent gain solutions. One possible research question would be to examine alternative optimization criteria, possibly based on independent eigenvalue excursions.

Secondly, the accurate modeling of many of the physical phenomena affecting rotor systems is presently an issue of uncertainty. These often highly nonlinear effects are generally treated by variable coefficients, the values of which may vary significantly from one effort to another. Of interest then, would be the sensitivity of a control application to variations in the modeling parameters.

Lastly, the dynamics associated with the control loop should be investigated as they affect high speed rotor systems. Delays from signal measurement, processing, and control actuators could greatly affect the performance of the control on machinery of this type.

LIST OF REFERENCES

1. W. J. Rankine, "Centrifugal Whirling of Shafts,"
    Engineer, April 9, 1869.

2. H. H. Jeffcott, "Lateral Vibration of Loaded
    Shafts in the Neighborhood of a Whirling Speed -
    The Effect of Want of Balance," Philosophical
    Magazine, Vol. 37, 1919, pp. 304-314.

3. F. F. Ehrich, "Identification and Avoidance of
    Instabilities and Self-Excited Vibrations in
    Rotating Machinery," ASME Paper No. 72-DE-21, New
    York, May 1972.

4. F. F. Ehrich, "Self-Excited Vibrations," Shock and
    Vibration Handbook, McGraw-Hill Inc., New York,
    1975.

5. D. W. Childs, "Fractional-Frequency Rotor Motion
    Due to Nonsymmetric Clearance Effects," ASME
    Journal for Power, July 1982, pp. 533-541.

6. "Effects of Bearing Deadband on Bearing Loads and
    Rotor Stability," Control Dynamics Company Final
    Report on NASA Contract No. NAS8-35050, January
    1984.

7. F. F. Ehrich, and J. J. O'Connor, "Stator Whirl
    with Rotors in Bearing Clearance," ASME Journal of
    Engineering Industry, August 1967, pp. 381-390.

8. H. Habermann, and G. L. Liard, "Practical Magnetic
    Bearings," IEEE Spectrum, September 1979,
    pp. 26-30.

9. G. Schweitzer, and R. Lange, "Characteristics
    of a Magnetic Rotor Bearing for Active Vibration
    Control," Institute of Mechanical Engineers
    Conference on Vibrations in Rotating Machinery,
    Cambrige, 1976, Paper No. C239/76.

10. V. Gondhalekar, and R. Holmes, "Design of Electromagnetic Bearing for Vibration Control of Flexible Transmission Shaft," NASA Conference Publication 2238, 1984, pp. 351-356.

11. C. R. Burrows, and M. N. Sahinkaya, "Control of Oil-Whirl by Pole Assignment," Proceedings of the American Controls Conference, 1984, pp. 354-359.

12. R. Stanway, and C. R. Burrows, "Active Vibration Control of A Flexible Rotor on Flexibly-Mounted Journal Bearings," Transactions of ASME, Journal of Dynamic Systems. Measurement, and Control, December 1981, pp. 383-388.

13. G. Schweitzer, "Stabilization of Self-Excited Rotor Vibrations by an Active Damper," Dynamics of Rotors. ed. F. I. Niordson, Springer-Verlag, New York, 1975, pp. 472-493.

14. G. Schweitzer, "Magnetic Bearings for Vibration Control," NASA Conference Publication 2409, 1985, pp. 317-326.

15. G. V.. Reklaitis, A. Ravindran, and K. M. Ragsdell, Engineering Optimization - Methods and Application. John Wiley and Sons, New York, 1983, pp. 87-98.